ARTICLES
https://doi.org/10.1038/s41556-019-0410-6
nature cell biology

In vivo generation of haematopoietic stem/progenitor cells from bone marrow-derived haemogenic endothelium

Laurent Yvernogeau[1,7], Rodolphe Gautier[1,9], Laurence Petit[1,9], Hanane Khoury[1], Frédéric Relaix[2], Vanessa Ribes[3], Helen Sang[4], Pierre Charbord[1], Michèle Souyri[1,8], Catherine Robin[5,6] and Thierry Jaffredo[1*]

It is well established that haematopoietic stem and progenitor cells (HSPCs) are generated from a transient subset of specialized endothelial cells termed haemogenic, present in the yolk sac, placenta and aorta, through an endothelial-to-haematopoietic transition (EHT). HSPC generation via EHT is thought to be restricted to the early stages of development. By using experimental embryology and genetic approaches in birds and mice, respectively, we document here the discovery of a bone marrow haemogenic endothelium in the late fetus/young adult. These cells are capable of de novo producing a cohort of HSPCs in situ that harbour a very specific molecular signature close to that of aortic endothelial cells undergoing EHT or their immediate progenies, i.e., recently emerged HSPCs. Taken together, our results reveal that HSPCs can be generated de novo past embryonic stages. Understanding the molecular events controlling this production will be critical for devising innovative therapies.

One of the major challenges in regenerative medicine is to reproduce tailor-made tissue-specific stem cells or early committed progenitors for cell replacement therapies. Despite recent progress[1,2], controlled production of bona fide haematopoietic stem and progenitor cells (HSPCs) from pluripotent precursors still requires a better understanding of where, when and how these cells are physiologically produced during development. It is now well established that HSPCs derive from a specialized subset of endothelial cells (ECs) designated as haemogenic through an endothelial-to-haematopoietic transition (EHT)[3–8]. EHT occurs early during embryogenesis in the main arteries of the embryo (such as the aorta)[9,10] to produce a few haematopoietic stem cells (HSCs), the founders of the adult haematopoietic system and a cohort of haematopoietic progenitors[11]. ECs undergoing EHT progressively round up, separate from their neighbours by breaking tight and adherens junctions, adopt a haematopoietic phenotype and eventually forming haematopoietic clusters in the vessel before detaching and leaving the haematopoietic site[12–14]. EHT is dependent on several intrinsic signalling pathways driven by key transcription factors (RUNX family transcription factor 1 (RUNX1), T cell acute lymphocytic leukemia 1 (TAL1), growth factor independent protein 1/1B (GFI1/GFI1B) and SRY-box 17 (SOX17))[15,16] and by extrinsic signals from the microenvironment (such as NOTCH, bone morphogenetic protein 4 (BMP 4), interleukin-3 (IL-3), wingless-related integration site (WNT), tumour necrosis factor-α (TNF-α) and others)[17,18]. Whether EHT occurs at later stages and in other organs (for example, bone marrow (BM)) is unknown. Here, we have discovered the existence of a haemogenic endothelium capable of de novo generation of HSPCs in the forming BM of chicken and mouse late fetuses and young adults. We identified the somite as the source of BM vascularization by tracing the BM-forming ECs through experimental embryology, genetic labelling and live imaging approaches and subsequently by analysing their haematopoietic progeny in adults. We demonstrated that the late fetal/young adult BM contains haemogenic ECs capable of producing HSPCs that are released into the blood circulation and colonize the secondary haematopoietic organs. Phenotypic and functional analyses showed that BM haemogenic endothelium-derived HSPCs are mainly multipotent progenitors (MPPs) and a few are HSCs. These cells harbour a specific molecular signature close to cells undergoing EHT or recently emerged HSPCs with a prominent Notch pathway, endothelial-specific genes and transcription factors involved in EHT. Our results demonstrate that HSPCs are de novo generated past embryonic stages. We therefore disclose a previously unappreciated haematopoietic wave occurring in the late fetal/young adult stage that fills the gap between the completion of embryonic haematopoiesis and the beginning of adult BM production. Identifying all steps of haematopoietic production and the molecular events controlling this process is of fundamental interest and might help to devise innovative stem cell therapies in the future.

Results

Existence of haemogenic ECs of somitic origin in chicken BM. To determine whether haemogenic ECs exist in the BM vascular network and also their potential origin, we used a combination of experimental embryology, genetic and transcriptomic approaches and functional analyses on chicken and mouse models. Based on previous research[19–22], the somite appeared to be a promising site of BM endothelial origin. The somite is a mesoderm-derived tissue that produces axial skeleton, muscles of the body wall and limbs, dermis

[1]IBPS, Laboratoire de Biologie du Développement CNRS UMR7622, Inserm U1156, Sorbonne Université, Paris, France. [2]Institut Mondor de Recherches Biomédicales, Créteil, France. [3]Institut Jacques Monod, Paris, France. [4]The Roslin Institute and R(D)SVS, University of Edinburgh, Edinburgh, UK. [5]Hubrecht Institute, Utrecht, Netherlands. [6]Regenerative Medicine Center, University Medical Center Utrecht, Utrecht, Netherlands. [7]Present address: Hubrecht Institute, Utrecht, Netherlands. [8]Present address: UMRS 1131, Institut Universitaire d'Hématologie, Hôpital Saint Louis, Paris, France. [9]These authors contributed equally: Rodolphe Gautier, Laurence Petit. *e-mail: thierry.jaffredo@upmc.fr

and endothelium[23]. Somite-derived ECs form the vascular network of the body wall, kidney and limbs[19–21]. To trace the endothelial derivatives of the somite in the chicken, we performed isotopic and isochronic grafts of green fluorescent protein (GFP)$^+$ chicken[24] presomitic mesoderm (PSM, the somite anlage) into wild-type (WT) chicken embryos at embryonic day (E)2 (15 somite pairs) (Fig. 1a). GFP$^+$ somite-derived cells were followed in individual grafted chickens ($n=34$) from the time of grafting (E2) to the adult stage by performing immunostaining and flow cytometry analyses on circulating blood, embryo sections or whole mount organs (Extended Data Table 1). A collection of endothelial/haematopoietic antibodies (MEP21)[25] or haematopoietic-specific antibodies against CD45 (PTPRC, pan-haematopoietic marker), CD41 (ITGA2B, HSPC marker)[26], c-Kit (CD117, HSPC marker), KUL1 (macrophage/monocyte marker) and CD3 (T cell marker) were used (Extended Data Table 1). In agreement with our previous work[20], PSM removal did not affect the aortic integrity (Extended Data Fig. 1a). Importantly, PSM did not contain either haematopoietic cells (HCs) or ECs, as demonstrated here by immunostainings and flow cytometry analyses on dissected individual PSMs (Extended Data Fig. 1b–d) or by polymerase chain reaction with reverse transcription (RT–PCR)[27]. It thereby rules out graft contamination by these two cell types later on during development.

Two days after grafting (at E4, $n=5$), PSM-derived GFP$^+$ cells were visible in the limb bud (Fig. 1b). GFP$^+$ cells were found around the neural tube, in limbs and the aorta. Of note, no GFP$^+$ cells were found within the intra-aortic clusters that harbour the first HSPCs (Fig. 1c–i), as expected from previous reports[19,20]. By E8, the grafted tissue had contributed to the body wall and limb muscle masses and to vascular ECs (Fig. 1j–l). No GFP$^+$ cells were found in the para-aortic foci ($n=2$) known to contain CD41$^+$ HSPCs[28] (Fig. 1m,n). These data therefore prove that GFP$^+$ cells do not contribute to the formation of the haematopoietic system at that stage, which is in keeping with the absence of GFP$^+$ circulating cells and with the established relationship between intra-aortic clusters and para-aortic foci[29]. The limb BM remained avascular until E12 ($n=2$), a stage when the first blood vessels associated with circulating CD41$^+$ and CD45$^+$ cells penetrate the cartilage tissue (Fig. 1o–r). No GFP$^+$ circulating blood cells were detected from E4 to E12 (Extended Data Fig. 2). The contribution of GFP$^+$ cells to the BM was extensively analysed at E16/E17, a developmental stage when sufficient BM cells could be observed or collected for flow cytometry analysis ($n=16$). Whole BM mounts showed the colonization of the grafted limb by GFP$^+$ cells (Fig. 2a) and the presence of a dense GFP$^+$ vascular network in the forming BM (Fig. 2b,c and Supplementary Video 1). A cross-section of the BM confirmed the presence of GFP$^+$ sinusoids, hence demonstrating the somite origin of the BM vascular network (Fig. 2d,e). Numerous GFP$^-$CD45$^+$ blood cells outside the GFP$^+$ vascular network were observed (Extended Data Fig. 3a–c). However, a subpopulation of GFP$^+$CD41$^+$, and to a lesser extent of GFP$^+$CD45$^+$ cells, was tightly associated with the GFP$^+$ sinusoids (Figs. 2f–i and 3a–f). The co-expression of blood cell markers and GFP (as shown on confocal sections) clearly demonstrated that a fraction of CD45$^+$ cells (Extended Data Fig. 3d–l and Supplementary Video 2) and CD41$^+$ cells (Fig. 3a–f and Supplementary Video 3) arose from GFP$^+$ somite-derived ECs in the BM. To ascertain the haematopoietic production in situ, we adapted the previously described time-lapse live confocal imaging[8] to thick slices of BM from E16/E17 grafted embryos that were stained with anti-CD41 antibodies. We were able to witness flat GFP$^+$CD41$^-$ ECs rounding up while expressing CD41$^+$ (as shown by CD41 staining after overnight imaging), therefore demonstrating the EHT (Supplementary Video 4 and Fig. 3g–j). At E16/E17, a small definite fraction of GFP$^+$ blood cells was found circulating (0.1–1%; Extended Data Fig. 2d). In the grafted limbs, GFP$^+$ cells represented an average of 1.10 ± 0.53% of the total BM mononucleated cells (Fig. 2j) that were found unevenly distributed among the endothelial and haematopoietic lineages. Strikingly, the GFP$^+$ cells significantly contributed to the BM haematopoietic production, representing 13.7 ± 7.3% of the CD41$^+$ cells, 3.0 ± 1.3% of c-Kit$^+$ cells, 7.4 ± 2.9% of CD3$^+$ cells and also to 14.2 ± 5.1% of the MEP21$^+$ population and 0.97 ± 0.52% of CD45$^+$ cells (Fig. 2k). On the other hand, 42.9 ± 5.4% of the GFP$^+$ cells were MEP21$^+$ ECs/HCs whereas 32.4 ± 10.4%, 28.4 ± 8.7%, 17.2 ± 4.7% and 5.0 ± 2.8% of the GFP$^+$ cells were CD45$^+$, CD41$^+$, c-Kit$^+$ or CD3$^+$, respectively (Fig. 2l and Extended Data Fig. 4a,b). Moreover, the MEP21$^+$CD45$^+$ population, known to be enriched in multipotent progenitors[25] and representing 2.4% of the mononucleated cells, harboured 15.2% of GFP$^+$ cells (Fig. 2m). Of note, no obvious difference was found in the haematopoietic composition of the BM between grafted (Extended Data Fig. 4a,b) and WT embryos (Extended Data Fig. 4c,d).

Long-term multilineage haematopoietic production from chicken BM haemogenic ECs. Long-term analysis of the grafted chicken embryos revealed that secondary haematopoietic organs were colonized by GFP$^+$ cells. For example, GFP$^+$ cells were visible in the thymic lobules of E16/E17 grafted recipients. GFP$^+$ cells were CD4$^+$ (1.4%), indicative of T cell differentiation (Extended Data Fig. 5a–e). Contrary to the BM, the vascular network of the thymus was not made by GFP$^+$ cells (Supplementary Video 5). A rather small but clear GFP$^+$ population was also present in the spleen (Extended Data Fig. 5f–h) and the bursa of Fabricius (Extended Data Fig. 5i–k), therefore supporting the multilineage contribution by the BM endothelium-derived HC population.

GFP chimeras were also examined at different time points post-hatching and analysed for the presence of GFP$^+$ cells associated with

Fig. 1 | Somite-derived ECs do not contribute to aortic haematopoiesis but are instrumental in the vascularization of the limbs and bones. a, Schematic depicting the isotopic and isochronic graft of a PSM from a ubiquitous GFP transgenic chicken embryo into a WT chicken embryo host. PSM grafts were performed at E2, at the level of somites 14–21[47,48]. **b**, E4-grafted embryo with GFP$^+$ somites and limb bud. **c**, Transverse section through the aorta, at mid-trunk level, of an E4-grafted embryo. MEP21 and GFP immunohistochemistry and Nomarski's interference contrast (Nom) merged signals. **d**, Enlarged view of the aortic floor in **c**. White arrows in **c** and **d** indicate haematopoietic clusters. **e**–**i**, Transverse section through the aorta of an E4-grafted embryo, at mid-trunk level, showing expression of MEP21 (**f**), CD45 (**g**), GFP (**h**) and DAPI (**i**), with a merged image (**e**). GFP$^+$ PSM-derived cells never contributed to haematopoietic clusters. **j**, E8-grafted embryo, transverse section, at mid-trunk level (MEP21 (red) and GFP (green) double staining). **k**,**l**, Higher magnification view of **j:** GFP staining (**k**) and MEP21 vascular staining (**l**). Wing bud vessels displayed both MEP21 and GFP staining, indicating that they originate from the graft. **m**,**n**, E8-grafted embryo, transverse section, at mid-trunk level (staining for CD41 (red), GFP (green) and DAPI (blue)). CD41$^+$ cells are found in the para-aortic foci (indicated by white arrows) close to the DC. **n** is a higher magnification of the box in **m**. CD41 and GFP do not overlap, indicating that intra-embryonic haematopoietic cells (HCs) do not derive from the grafted PSM. **o**–**r**, Sagittal section of an E12-grafted limb, showing onset of bone marrow colonization: GFP and DAPI staining (**o**) and higher magnification views of **o** (**p**–**r**). **p**, MEP21 and GFP staining, showing partial overlap of markers, with MEP21 weakly expressed in EC progenitors. **q**, Same area, adjacent section: staining for GFP and DAPI. **r**, CD45, GFP and DAPI staining, adjacent section; CD45$^+$GFP$^-$ cells invade the cartilage area. LB, limb bud; Ao, aorta; C, cartilage; DC, duct of Cuvier; FB, feather bud; G, gut; NT, neural tube; M, muscle; V, vessel. Scale bars: 200 µm (**b**); 30 µm (**c**); 20 µm (**d**); 35 µm (**e**–**i**); 250 µm (**j**,**m**); 350 µm (**k**,**l**); 150 µm (**n**); 400 µm (**o**); 70 µm (**p**,**q**); 50 µm (**r**). Images are representative of five (**b**–**i**) and two embryos (**j**,**o**–**r**).

endothelial and haematopoietic lineages in the BM ($n=7$, up to 41 weeks; Fig. 4a,b and Extended Data Table 1). The continued presence of GFP$^+$ cells in the BM (Fig. 4c), and a rather similar distribution of GFP among the endothelial and haematopoietic fractions (Fig. 4d,e and Extended Data Fig. 6a–d) compared to E16/E17 embryos (Fig. 2j–m and Extended Data Fig. 4), were found in the growing chicken. The MEP21$^+$CD45$^+$ population harboured 6.1% of GFP$^+$ cells (Fig. 4f). Fluorescence activated cell sorting (FACS)

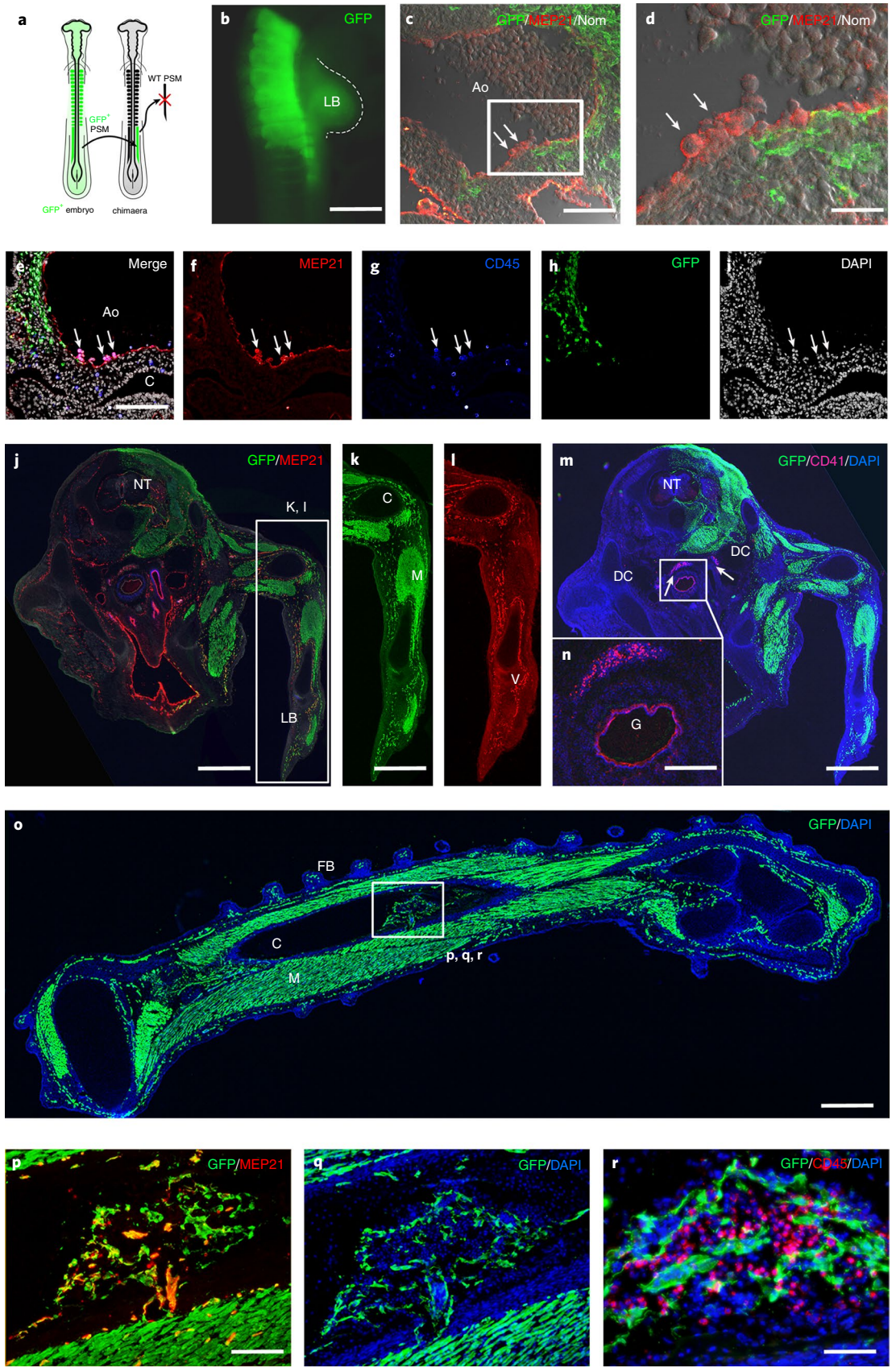

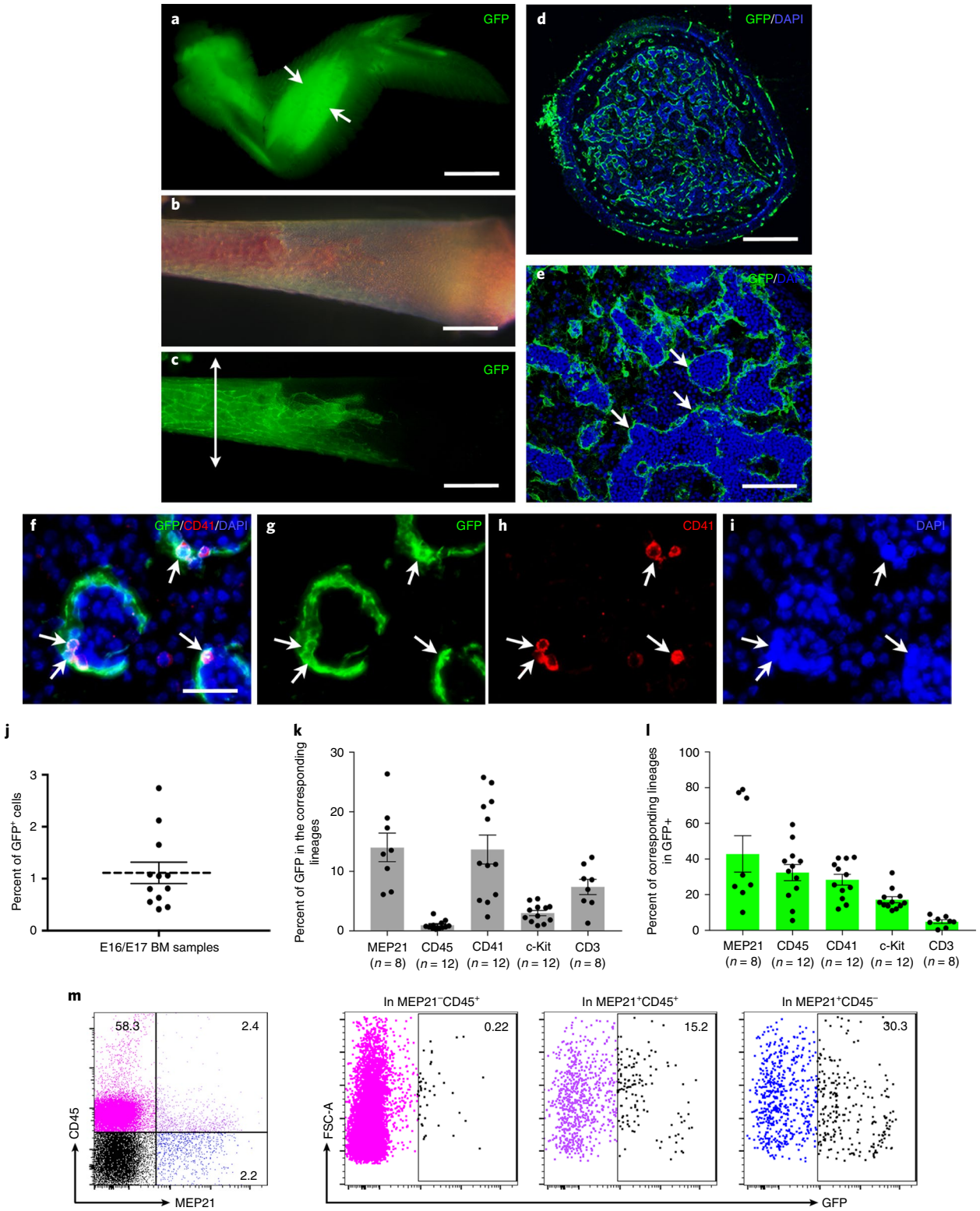

Fig. 2 | The chicken BM vascular network derives from the somite and produces a cohort of HSPCs during late embryonic life. a, E16/E17 limb colonized by GFP+ somite-derived cells that have formed visible muscle masses (arrows). **b**,**c**, Isolated radius showing conspicuous signs of BM haematopoiesis observed under visible (**b**) or ultraviolet illumination (**c**). GFP tubule-like structures were observed in the BM. The arrow indicates the level of section seen in **d**. **d**,**e**, Representative cross-section (arrow in **c**) through the bone stained for DAPI (cell nuclei) and GFP showing GFP+ cells forming sinusoids (white arrows). **f**–**i**, Representative fluorescent images showing the co-distribution of GFP+ sinusoids (**g**) and CD41+ HCs (**h**) (arrows), counterstained with DAPI (**i**). A merged image is shown in **f**. **j**, Percentage of GFP+ cells in E16/E17 grafted limbs. Each dot represents a grafted recipient (n=12 chicken). **k**, Distribution of GFP+ cells in the endothelial and haematopoietic lineages. **l**, Distribution of the endothelial and the different haematopoietic lineages within the GFP+ population. Numbers in brackets (**k**,**l**) are the numbers of grafted recipients n. **m**, Representative flow cytometry analysis (12 independent animals) identifying the MEP21+CD45+ population known to be enriched in multipotent progenitors[25] and the contribution of the GFP+ PSM-derived cells to the endothelial and/or haematopoietic (multipotent) progenitors. Data are presented as mean ± s.e.m. Scale bars: 1 cm (**a**); 300 µm (**b**,**c**); 200 µm (**d**); 80 µm (**e**); 15 µm (**f**-**i**).

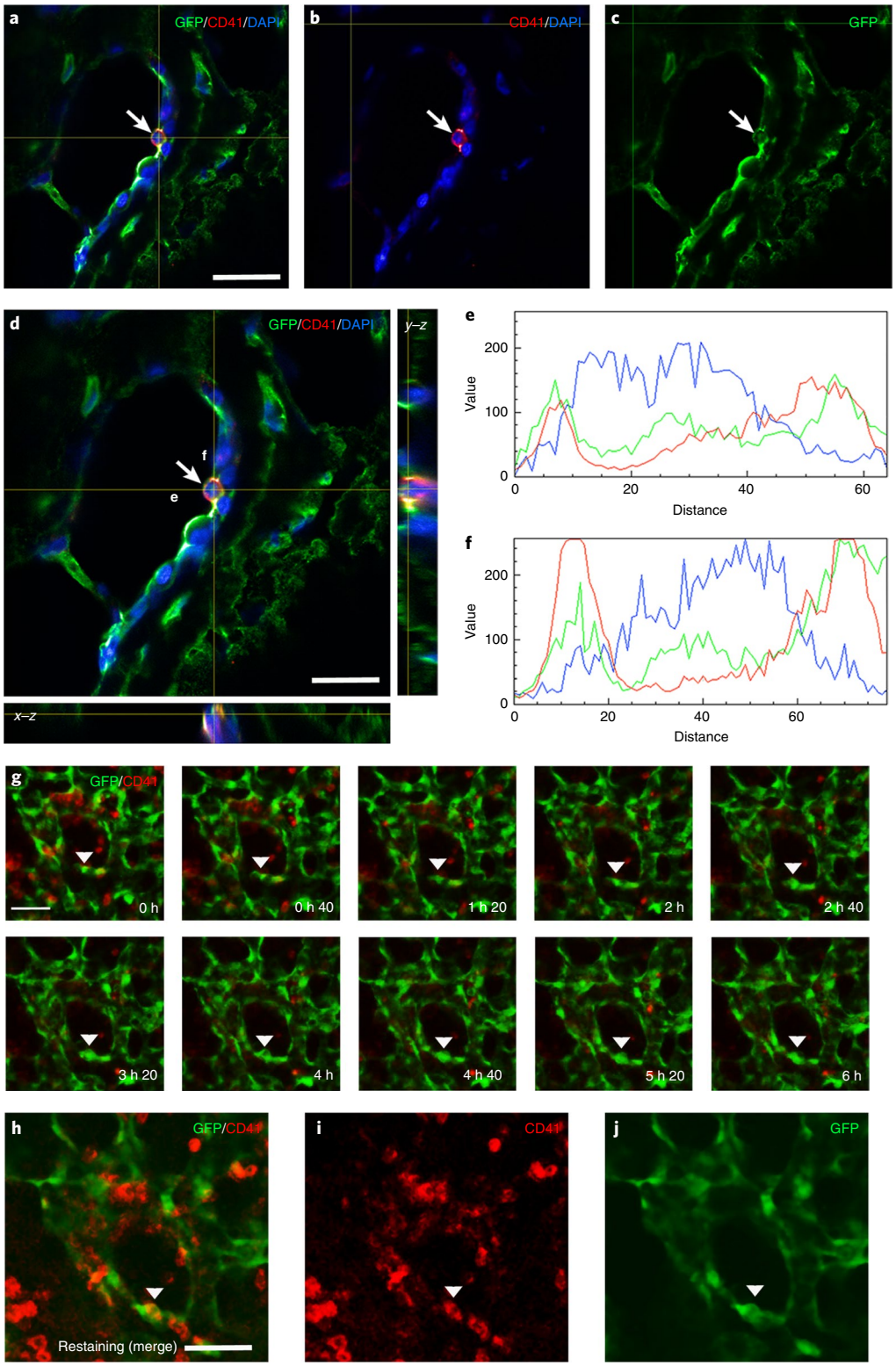

Fig. 3 | Emergence of CD41⁺ haematopoietic progenitors from GFP⁺ ECs in the BM. a-c, Confocal section of E16 BM after GFP, CD41 and DAPI (nucleus) staining. The arrow points to a CD41⁺GFP⁺ cell attached to the GFP⁺ vessel. **a**, merge of GFP, CD41 and DAPI. **b**, CD41 and DAPI double staining. **c**, GFP fluorescence. **d**, Enlarged view of the image in **a**. The two yellow lines indicate the *x* and *y* axes. The right stripe represents the *y*–*z* view and the bottom stripe represents the *x*–*z* view. **e**,**f**, RGB colour profiles of the *y*–*z* (**e**) and *x*–*z* (**f**) views, showing that CD41 and GFP profiles are superposed, indicating that both markers are within the same cell (three independent embryos). The distance is given in pixels. **g**, Time-lapse imaging of a transversal section of E16-grafted BM showing the progressive emergence of a GFP⁺CD41⁻ cell from the endothelium of a blood vessel. Time is shown in hours and minutes. **h**, After time-lapse imaging (**g**) the section was stained again with anti-CD41-PE antibodies. **i**,**j**, The newly emerged GFP⁺ cell (**j**) expressed CD41 (**i**) (there was no CD41 expression at the beginning of the imaging). Scale bars: 20 µm (**a-c**); 25 µm (**d**); 5 µm (**g**-**j**). Images represent 10 independent experiments (**a**–**d**), with two animals in independent experiments (**h**–**j**), five sections per slide.

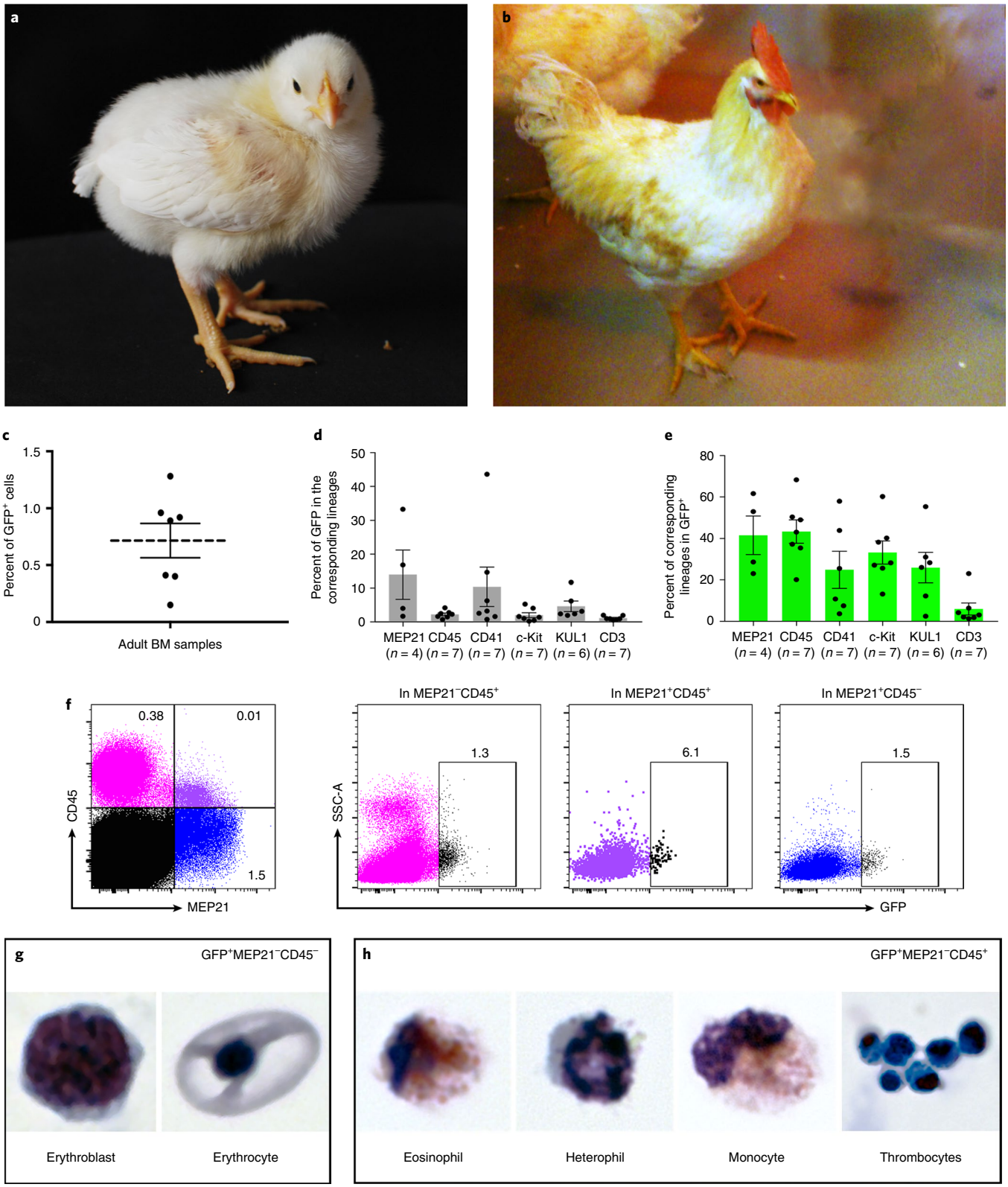

Fig. 4 | HSPCs derived from the late fetal BM endothelium persist after hatching. a,**b**, PSM-grafted chimaeras at eight days (**a**) and five months (**b**) post grafting (seven independent hatched animals). **c**, Percentage of GFP$^+$ cells in grafted limbs at five months. Each dot represents a grafted recipient ($n = 7$ chickens). **d**, Distribution of GFP$^+$ cells in the different BM endothelial and haematopoietic lineages of a 5.5-month-old recipient. **e**, Distribution of the BM endothelial and haematopoietic lineages contained in the GFP$^+$ population. Numbers in brackets under the *x* axes in **d** and **e** indicate the numbers of analysed transplanted recipients. **f**, Combined flow cytometry analysis of the adult grafted BM for MEP21 and CD45 populations showing the percentages of MEP21$^-$CD45$^+$, MEP21$^+$CD45$^+$ and MEP21$^+$CD45$^-$ populations and the contribution of GFP$^+$ cells within each population. **g**,**h**, May–Grünwald–Giemsa staining of sorted adult GFP$^+$MEP21$^-$CD45$^-$ (**g**) and GFP$^+$MEP21$^-$CD45$^+$ (**h**) cells. All data are presented as mean ± s.e.m. SSC, side scatter.

followed by cytospin and May–Grünwald–Giemsa staining of the GFP$^+$MEP21$^-$CD45$^-$ cell fraction disclosed an erythroblast/erythrocyte population (Fig. 4g), whereas the GFP$^+$MEP21$^-$CD45$^+$ fraction displayed eosinophils, heterophils, monocytes and thrombocytes (Fig. 4h). The data therefore demonstrate that chicken BM haemogenic ECs produce multilineage HCs capable of colonizing secondary haematopoietic tissues in the long term.

Somite-derived ECs give rise to MPP-3 and HSCs in the BM of the late fetus/young adult mice through an EHT. To assess whether the process of haematopoietic production by somite-derived BM haemogenic ECs disclosed in birds is conserved in mammals, two mouse models were used. The contribution of the somite to the perinatal BM was traced by using Pax3$^{CRE/+}$ mice crossed to ROSA$^{mT/mG}$ mice. We first assessed that no Pax3$^+$ cells were present in the embryonic aorta at E10.5, when the first HSPCs emerge (Extended Data Fig. 7a,b). Similar to the chicken, ECs and HCs associated with GFP expression were found in E19 to E21 fetal BM. The presence of mature cells from different haematopoietic lineages (CD45$^+$, CD3$^+$, B220$^+$, Gr1$^+$, CD11b$^+$, Ter119$^+$), HSPCs (Sca1$^+$c-Kit$^+$, CD144$^+$CD45$^+$) and ECs (CD144$^+$CD45$^-$) were analysed in the perinatal mouse BM (Extended Data Fig. 7c; $n=3$). Moreover, the distribution of GFP$^+$ cells in each population was measured (Extended Data Fig. 7d; $n=3$). GFP$^+$ cells contributed to all lineages. However, the highest contribution was found in the CD3$^+$ T cell population, the CD144$^+$CD45$^+$ population that is similar to the first HSPCs emerging from the aorta[30], and the Sca1$^+$c-Kit$^+$ HSPC population (Extended Data Fig. 7d–g). These results were highly significant compared to control samples (Extended Data Fig. 7h). BM mononucleated cells contained an average of 0.30 ± 0.02% GFP$^+$ cells (Extended Data Fig. 7e), in line with the numbers found in birds (Figs. 2j and 4c), with 4.2 ± 1.2% of CD144$^+$CD45$^+$ cells expressing GFP (Extended Data Fig. 7d,f). The rare Sca1$^+$c-Kit$^+$ population displayed a conspicuous fraction of GFP$^+$ cells (4.5 ± 2.1%; Extended Data Fig. 7g), indicating the production of HSPCs by somite-derived BM haemogenic endothelium.

To further specifically trace the progeny of ECs in the long term after birth, we used an indelible marking system to target the endothelium. For this purpose, floxed reporter yellow fluorescent protein (YFP) transgenic mice[31] were crossed to mice with a tamoxifen-inducible Cre driven via the complete endothelial-specific VE-cadherin (CDH5) upstream regulatory sequences[32]. Day (D)1 pups received one injection of 50 µg tamoxifen every day for three days (Fig. 5a). BMs were then analysed at different time points up to 15 weeks (105 days) for the presence of YFP$^+$ ECs and HCs ($n=2$–6). Importantly, no CD45$^+$ cells displayed YFP expression immediately after the last tamoxifen injection ($n=11$), ruling out contamination from haematopoietic progenitors expressing CD144 (Extended Data Fig. 8a). D27 BM analysis uncovered the presence of 0.096 ± 0.011% YFP$^+$ cells in total mononucleated cells (Fig. 5b). HCs (4.1 ± 0.4% of CD144$^+$CD45$^+$ and 0.0054 ± 0.0013% of CD144$^-$CD45$^+$) and ECs (42.4 ± 6.8% of CD144$^+$CD45$^-$) were YFP$^+$ (Fig. 5c). The stainings were accurate regarding the absence of YFP staining observed in the non-induced animals (Extended Data Fig. 8b). Following up the YFP$^+$ population, we observed that CD144$^+$CD45$^-$ ECs and the rare lineage-negative Sca1$^+$c-Kit$^+$ (LSK) HSPCs decreased over time to reach almost zero 105 days after birth, indicating a progressive disappearance of the haemogenic endothelium and haematopoietic production with age (Fig. 5d). Of note, tamoxifen inductions at later stages after birth resulted in a reduced number of YFP$^+$ CD144$^+$CD45$^-$ cells and LSK cells, confirming the progressive loss of haemogenic endothelium with age (Extended Data Fig. 8d,e). Aiming to better identify the immature YFP$^+$ cell population, we analysed LSK cells using the SLAM family markers known to distinguish HSCs from MPPs[33] (Fig. 5e). We disclosed the presence of 7.8 ± 1.6% of YFP$^+$ cells in the LSK population (Fig. 5e). YFP$^+$ cells were highly enriched in the CD150$^-$CD48$^-$ MPP fraction[34] (23.1 ± 4.7%) and were also present in the CD150$^+$CD48$^-$ HSC fraction (5.0 ± 1.6%) (Fig. 5e,f). Further analysis using CD229 and CD244 markers[33] to hierarchically discriminate the different MPP populations revealed the presence of 65.3 ± 8.9% YFP$^+$ cells in the CD150$^-$CD48$^-$CD229$^+$CD244$^+$ MPP-3 fraction that represents transiently reconstituting haematopoietic progenitors, and to a lesser extent in the MPP-1 population that represents intermediate and transiently reconstituting progenitors (5.9 ± 4.2%, Fig. 5g). Comparison of the YFP$^-$ and YFP$^+$ LSK cell fractions using the SLAM code revealed that the three cell subsets HPC-1, HPC-2 and HSC were decreased in YFP$^+$ versus YFP$^-$ cells (for HPC-1 0.30 ± 0.05% versus 64.4 ± 1.16%; for HPC-2, 0.1 ± 0.03% versus 4.5 ± 0.5%; for HSC 2.6 ± 0.44% versus 7.8 ± 0.33%). MPPs were, however, strongly increased in YFP$^+$ versus YFP$^-$ cells (97 ± 0.4% versus 23.2 ± 1.4%; Fig. 5h). YFP$^+$ cells displayed a low percentage of MPP-1 and MPP-2 (0.1 ± 0.02% and 0.52 ± 0.12%, respectively) compared to YFP$^-$ cells (1.8 ± 0.23% and 92.4 ± 1%, respectively) and a high percentage of MPP-3 (62.7 ± 4%) compared to YFP$^-$ cells (4.2 ± 0.3%) (Fig. 5h). Hence, YFP$^+$ cells contained mostly MPP-3, that is, transiently reconstituting multipotent progenitors and a few HSCs. Again, this staining was accurate when compared to non-induced animals (Extended Data Fig. 8c).

To further analyse whether ECs of the forming mouse BM were endowed with haemogenic potential we adapted to the mouse model an in vitro test we previously used to demonstrate EHT in quail embryo cells[27]. In addition to the cytokines and growth factors already present in the medium (see Methods), we added murine IL-3, FMS-like tyrosine kinase 3 ligand (FLT3L), stem cell factor (SCF) and thrombopoietin (TPO). We performed three independent experiments with eight-day-old mouse BM cells ($n=6$ pooled mice per experiment) and seeded 10 to 15,000 cells per well. CD144$^-$CD45$^+$ HCs or CD144$^+$CD45$^-$ ECs were seeded in culture and followed daily over a period of four days (Extended Data Fig. 9a). As expected, the CD144$^-$CD45$^+$ fraction exhibited conspicuous (98.6 ± 0.6%) haematopoietic production (Extended Data Fig. 9b,e).

Fig. 5 | Conditional expression of YFP in VE-cadherin cells in BM at birth discloses a contribution of vascular ECs to MPPs and Lin$^-$Sca1$^+$c-kit$^+$CD150$^+$CD48$^-$ HSCs. a, Scheme showing the activation of VE-cadherin (CD144, CDH5) by tamoxifen injection and the different time points of analysis. Bottom arrows, time of tamoxifen injections. Top arrows, time points of analyses. Data are from five independent tamoxifen induction experiments. The numbers of analysed animals per time point are indicated in red above the timeline. **b**, YFP expression in mononucleated BM cells at 27 days (12 mice, four independent experiments). **c**, Representative flow cytometry analysis of CD144$^-$CD45$^+$, CD144$^+$CD45$^+$ and CD144$^+$CD45$^-$ populations and YFP expression in each population (12 mice, four independent experiments). **d**, Time course analysis of total YFP$^+$ cells, YFP$^+$ cells in CD144$^+$CD45$^-$ and LSK populations. $n=12$ mice. Data are presented as mean ± s.e.m. **e**–**g**, Representative flow cytometry analyses of the SLAM/LSK cells (eight mice, three independent experiments) (**e**), HSCs (eight mice, three independent experiments) (**f**) and MPPs (five mice, two independent experiments) (**f**,**g**) revealed an enrichment of YFP$^+$ cells in the MPP-3 fraction and in HSCs. **h**, Differences between YFP$^-$ (upper panels) and YFP$^+$ cells (lower panels) regarding the expression of the SLAM receptors. Lin$^-$ cells constitute 95.4 ± 0.5% and 37.4 ± 0.6% of the YFP$^+$ and YFP$^-$ cell fractions, respectively. Sca1$^+$c-Kit$^+$ (CD117) cells constitute 55.7 ± 1.1% and 1.1 ± 0.035% of the YFP$^+$ and YFP$^-$ cell fractions, respectively. The combination of CD150 and CD48 markers reveals a strong enrichment in MPP in the YFP$^+$ cells (97 ± 0.4% versus 23.2 ± 1.4% in YFP$^-$ cells). The combination of CD229 and CD244 markers reveals a strong enrichment in MPP-3 in the YFP$^+$ versus YFP$^-$ cells (62.7 ± 4.4% versus 4.2 ± 0.3%, five mice in two independent experiments).

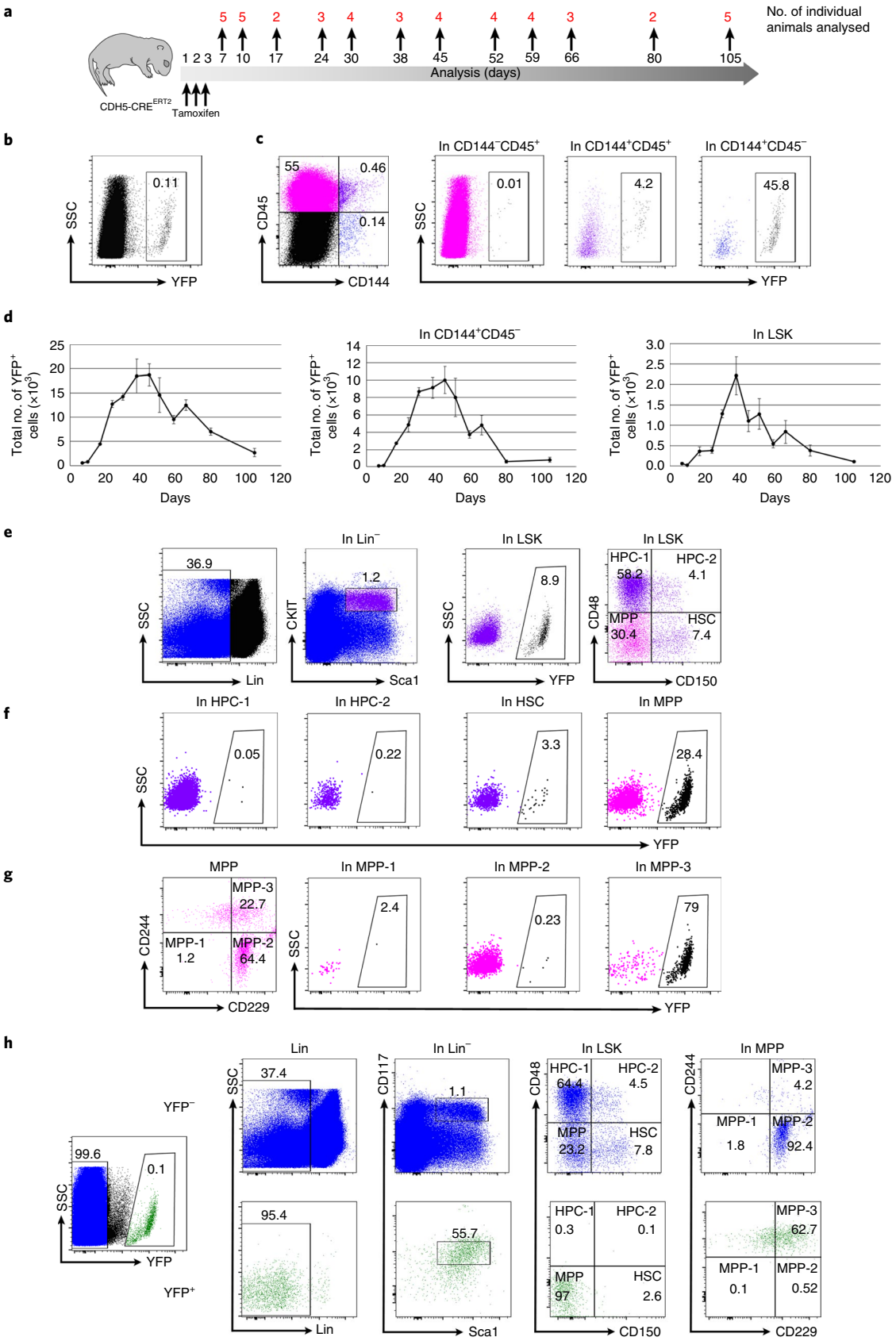

Importantly, the CD144⁺CD45⁻ fraction produced round cells that either remained attached to flat adherent cells (Extended Data Fig. 9c) or were found floating in the medium (Extended Data Fig. 9d). Flow cytometry analysis showed that these cells expressed the haematopoietic marker CD45 (34.9 ± 12%, Extended Data Fig. 9f), demonstrating that these cells are also capable of EHT in vitro.

HCs from BM haemogenic endothelium share a molecular signature with newly born HCs and ECs of the embryonic aorta. To identify at the molecular level the HCs originating from a VE-cadherin ancestor, we performed transcriptomic analysis on LSK YFP$^-$ and YFP$^+$ cells isolated from D27 BM. Principal component analysis (PCA) on the entire set of 30,922 genes indicated a clear-cut distinction between LSK YFP$^+$ and LSK YFP$^-$ cells (Extended Data Fig. 9g and Supplementary Table 1). Gene ontology (GO) using the database DAVID (http://david.ncifcrf.gov) performed on genes upregulated in the two populations (using analysis of variance (ANOVA) with $P \leq 0.03$, giving 1,417 and 1,552 genes in the LSK YFP$^+$ and YFP$^-$ fractions, respectively) disclosed differentially represented GO categories (Extended Data Fig. 9h). While GO categories for LSK YFP$^-$ cells concerned the broad machinery of transcription, translation and cell cycle and DNA repair, categories for LSK YFP$^+$ cells were focused on extracellular matrix (ECM)-to-actin cytoskeleton interactions, including membrane, ECM, focal adhesion and actin-binding proteins. To determine more accurately the identity of the LSK YFP$^+$ cells, we included transcriptomes of several BM and aorta-gonads-mesonephros (AGM)-derived EC and HC types (that is, BM lin$^+$ HCs, BM LSK CD150$^+$CD48$^-$ HSCs, AGM CD144$^+$CD45$^-$ ECs, AGM CD144$^-$CD45$^+$ HCs and AGM CD144$^+$CD45$^+$ HSPCs together with LSK YFP$^+$ and YFP$^-$ cells, $n = 23$ samples). PCA analysis on the whole gene set (18,920 genes) revealed three main groups (Fig. 6a, upper panel). The first group, on the left-hand side of the figure, included BM and AGM HCs; the second group, on the right-hand side, included adult and embryonic HSPCs (BM LSK CD150$^+$CD48$^-$, AGM CD144$^+$CD45$^+$ and LSK YFP$^-$ cells); and the third group, on the bottom, included AGM ECs and LSK YFP$^+$ cells. Further analysis was performed on differentially expressed genes (DEGs) identified by ANOVA (with $P \leq 0.001$, giving 986 up- and 1,070 downregulated genes). PCA using the 23 samples and the set of 2,056 DEGs helped identify four clusters (encircled in Fig. 6a, lower panel), which were confirmed by hierarchical clustering (Extended Data Fig. 9i). The first component, representing 51.7% of the variance, corresponded to the contrast between LSK YFP$^+$ (left) and LSK YFP$^-$ (right) cells, as expected. The second helped discriminate HCs (bottom) from the remaining cells (top). To uncover how DEGs were interrelated within the two LSK YFP$^+$ and LSK YFP$^-$ cell populations, we performed a weighted gene correlation network analysis (WGCNA)[35], which disclosed two major gene modules (sub-networks). The yellow and black modules, whose eigengenes were either negatively or positively correlated to the trait (that is, the contrast between LSK YFP$^+$ and YFP$^-$ cells) corresponded to genes upregulated in LSK YFP$^+$ and YFP$^-$ cells, respectively (Fig. 6b). GO analysis of the two gene sets revealed strong differences in their biological functions. The LSK YFP$^-$ network contained genes related to cell proliferation (cell cycle, DNA replication, protein translation and folding and mRNA splicing). The LSK YFP$^+$ module was enriched in molecules implicated in the ECM-to-actin cytoskeleton interaction and pertaining to the bone morphogenetic protein (BMP) and Notch signalling pathways (Fig. 6c). A close-up view of the genes within the LSK YFP$^-$ module revealed the presence of a core of transcription factors including key regulators of haematopoiesis, such as *Hoxa9*, *Meis1*, *Hlf* and *Etv6* (Fig. 6d, left). Within the LSK YFP$^+$ module the presence of several Notch genes, from canonical (Notch4, Dll4) and non-canonical (Mamld1) pathways, as well as many endothelial genes such as *Pecam1*, *Kdr*, *Flt1*, *Flt4* and also *Cdh5*, *Aplnr* and *Emcn* (Fig. 6d, right), was a compelling argument for the endothelial origin of LSK YFP$^+$ cells. We finally tested the HSC potential of the LSK YFP$^+$ and YFP$^-$ cells using transplantation experiments into irradiated recipients. LSK YFP$^-$ cells contributed to a robust, multilineage haematopoiesis (Fig. 6e). Remarkably, LSK YFP$^+$ cells also contributed, albeit to a lesser extent, to multilineage haematopoiesis, with a preferential differentiation towards the lymphoid and erythroid lineages (Fig. 6e,f and Extended Data Fig. 10). Overall, our data demonstrate that the HC population produced from the BM haemogenic endothelium contains MPP-3 and HSCs that have a similar molecular signature to the ECs and newly formed HSPCs produced in the embryonic aorta.

Discussion

Our cell tracing studies have identified a yet unappreciated wave of haematopoiesis (MPP-3 and HSCs) occurring de novo in the BM of the late fetus/young adult from resident haemogenic ECs of somite origin in both chicken and mouse species. Previous tracing experiments in chicken and mouse identified two sources of ECs: (1) the splanchnic mesoderm, which gives rise to ECs vascularizing the viscerae, forming the double primitive aortic anlage[36] and endowed with a dual endothelial and haematopoietic potential that is haemogenic[37]; (2) the somites, which produce pure ECs that contribute the entire endothelial network of the body wall and limbs[19–22,38,39]. Haematopoiesis in the aorta relies on splanchnic ECs located in the aortic floor, whereas the aortic roof is made of somite-derived ECs lacking haemogenic potential[19,20], hence contributing to the polarization of the vessel[20]. Somite-derived ECs never give rise to haematopoiesis in situ, but can acquire a haemogenic potential upon treatment with ventralizing factors such as vascular endothelial growth factor or basic fibroblast growth factor or a transient treatment with endoderm[37]. Our hypothesis is that the forming BM provides a microenvironment that allows somite-derived ECs to acquire a transient haemogenic potential and give rise to haematopoiesis. Interestingly, somite-derived ECs were shown to be instrumental in triggering aortic haematopoiesis from resident

Fig. 6 | BM vascular EC-derived HSPCs display an endo-haematopoietic transcriptomic profile and show long-term multilineage reconstitution. **a**, Upper panel: PCA, 23 samples, entire gene set (18,920 genes). Lower panel: PCA, 23 samples, 2,056 DEGs (986 up, 1,070 down). Gene set obtained by ANOVA (YFP$^+$ versus YFP$^-$, $P < 0{,}001$). PC1 corresponds to contrast between YFP$^+$ and YFP$^-$ cells. **b**, Module detection by clustering using the topological overlap matrix (TOM) and merged dynamic tree cut method. Same as for **a**, lower panel. Parameters: power, 26; adjacency, signed; correlation, Pearson's; linkage, average; minimum module size, 30. Two major yellow and black modules, whose eigen genes are positively and negatively correlated to the YFP$^+$ to YFP$^-$ cell contrast, are highlighted. **c**, GO categories corresponding to genes in the yellow and black modules. Enrichment scores are as given by the DAVID database. **d**, Cytoscape connectivity plot of yellow (upregulated in YFP$^+$ cells) and black (upregulated in YFP$^-$ cells) modules. The most connected genes are shown (188/447 for the yellow module; 282/829 for the black module). **e**, Comparison of levels of circulating blood cells analysed following engraftment between recipients transplanted with LSK YFP$^+$ or YFP$^-$ cells. Empty triangles, LSK YFP$^-$ cells grafted in $n = 6$ animals. Black circles, LSK YFP$^+$ cells grafted in $n = 4$ animals. Bars represent means. **f**, Flow cytometry analysis of a C57BL/6-CD45.1 recipient injected with 2,000 LSK YFP$^-$ (left plots) or YFP$^+$ (right plots) cells (C57Bl6-CD45.2). Right plots: YFP expression in engrafted CD45.2$^+$ populations. Experiments were repeated twice. **g–i**, Location and fate of PSM (green) and lateral plate mesoderm (LPM, blue) at representative and equivalent time points during chicken and mouse development: PSM and LPM in E1.5 chicken and E9.5 mouse embryos (**g**) (LPM: mesoderm located laterally and ventrally to the PSM); the PSM subdivides into somites, which give rise to muscles, vasculature and bones (**h**) and the haemogenic ECs of the aorta and associated haematopoietic cluster (IAHC) cells derive exclusively from the LPM; in young adults, bones and marrow derive from the LPM and vasculature from the PSM (**i**) (most HSPCs originate from LPM-derived HSCs or de novo from PSM-derived endothelium of the bone marrow).

haemogenic ECs in zebrafish[40]. Also, a recent report suggested the existence of a cell subset within the somite that is endowed with a haematopoietic potential[41].

It is known that the yolk sac produces two partially overlapping waves of haematopoiesis. The first, designated as primitive, gives rise to erythroid, megakaryocytes and macrophage progenitors

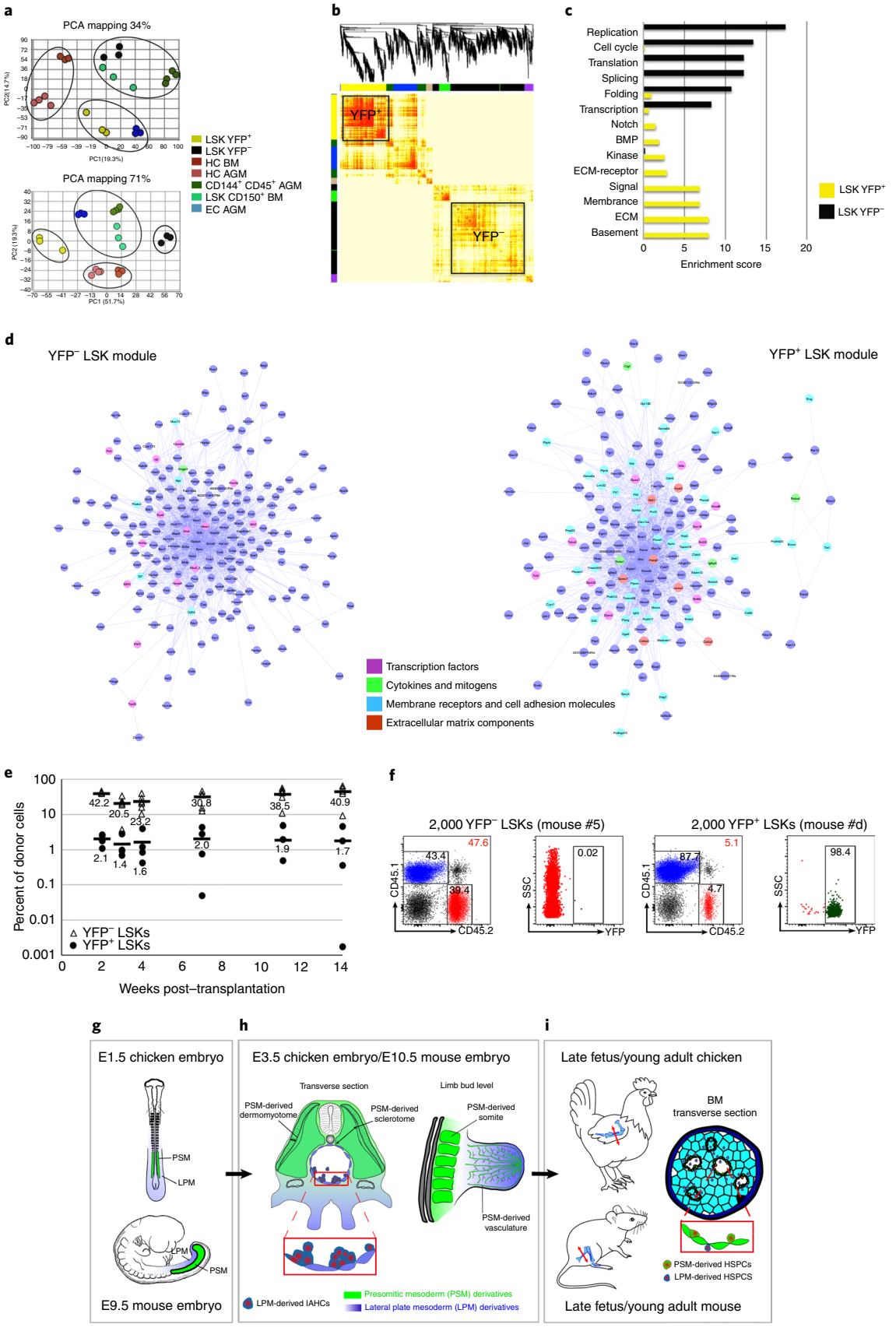

that rapidly mature into the blood stream. The second, designated as definitive, produces erythroid, megakaryocyte, macrophage, neutrophil and mast cell progenitors that seed the fetal liver and trigger haematopoiesis[42]. These progenitors are sufficient for the mouse embryo to survive until birth, when the AGM-derived HSC-dependent wave will take over[42,43]. One may speculate that the transient haematopoietic production discovered in our study fills the gap between the end of the yolk sac haematopoiesis and the BM HSC-dependent production. Indeed, the pool of HSCs that expanded in the fetal liver starts to colonize the BM at E17[44]. Because BM colonization is low and HSCs are present in very few numbers at birth, some time might be required before HSCs find their final adult-type niches and start to differentiate/proliferate into more committed progenitors and mature blood cells. This transient haematopoietic wave might also prepare the BM niches to mature to an appropriate state to accommodate HSCs amplified in the fetal liver. Such hypotheses will need to be verified in the future. Interestingly, a transient HSC population harbouring robust adult haematopoietic reconstitution potential (lymphoid biased) was recently uncovered during mouse embryonic life[45]. A recent paper indicated that yolk sac-derived erythromyeloid progenitors may contribute to the intraembryonic vascular endothelium, where they persist until adulthood, unravelling an unexpected source of ECs[46]. In our approaches, PSM does not contain erythromyeloid progenitors, ruling out a contribution of this cell type to HSPC formation by the BM. This, together with our findings, emphasizes an unappreciated complexity of the ontogeny of the haematopoietic system. In our experiments, it is highly unlikely that the GFP$^+$ cells that we observed came from another organ. We never detected GFP$^+$ intra-aortic haematopoietic clusters, nor GFP$^+$ cells in the para-aortic foci or circulating before the establishment of the BM. Moreover, the BM is the main haematopoietic organ and is therefore the most likely site where EHT could take place. Based on the timing of tamoxifen induction in mice, a contribution of the fetal liver is highly unlikely. A model of cell origins and lineage relationships in both chicken and mouse species is displayed in Fig. 6g–i. Overall, our study has proved that HSPCs could be produced in the BM through a haemogenic endothelium intermediate past the yolk sac and embryonic aorta stages; this is important information that should help in the design of therapies for haematopoietic disorders.

Online content

Any methods, additional references, Nature Research reporting summaries, source data, extended data, supplementary information, acknowledgements, peer review information; details of author contributions and competing interests; and statements of data and code availability are available at https://doi.org/10.1038/s41556-019-0410-6.

Received: 6 November 2018; Accepted: 23 September 2019;
Published online: 4 November 2019

References

1. Sugimura, R. et al. Haematopoietic stem and progenitor cells from human pluripotent stem cells. *Nature* **545**, 432–438 (2017).
2. Lis, R. et al. Conversion of adult endothelium to immunocompetent haematopoietic stem cells. *Nature* **545**, 439–445 (2017).
3. Jaffredo, T., Gautier, R., Eichmann, A. & Dieterlen-Lievre, F. Intraaortic hemopoietic cells are derived from endothelial cells during ontogeny. *Development* **125**, 4575–4583 (1998).
4. Zovein, A. C. et al. Fate tracing reveals the endothelial origin of hematopoietic stem cells. *Cell Stem Cell* **3**, 625–636 (2008).
5. Chen, M. J., Yokomizo, T., Zeigler, B. M., Dzierzak, E. & Speck, N. A. Runx1 is required for the endothelial to haematopoietic cell transition but not thereafter. *Nature* **457**, 887–891 (2009).
6. Kissa, K. & Herbomel, P. Blood stem cells emerge from aortic endothelium by a novel type of cell transition. *Nature* **464**, 112–115 (2010).
7. Swiers, G., Rode, C., Azzoni, E. & de Bruijn, M. F. A short history of hemogenic endothelium. *Blood Cells Mol. Dis.* **51**, 206–212 (2013).
8. Boisset, J. C. et al. In vivo imaging of haematopoietic cells emerging from the mouse aortic endothelium. *Nature* **464**, 116–120 (2010).
9. Mikkola, H. K. & Orkin, S. H. The journey of developing hematopoietic stem cells. *Development* **133**, 3733–3744 (2006).
10. Dzierzak, E. & Speck, N. A. Of lineage and legacy: the development of mammalian hematopoietic stem cells. *Nat. Immunol.* **9**, 129–136 (2008).
11. Yokomizo, T. & Dzierzak, E. Three-dimensional cartography of hematopoietic clusters in the vasculature of whole mouse embryos. *Development* **137**, 3651–3661 (2010).
12. Boisset, J. C. & Robin, C. On the origin of hematopoietic stem cells: progress and controversy. *Stem Cell Res.* **8**, 1–13 (2012).
13. Drevon, C. & Jaffredo, T. Cell interactions and cell signaling during hematopoietic development. *Exp. Cell Res.* **329**, 200–206 (2014).
14. Dejana, E., Hirschi, K. K. & Simons, M. The molecular basis of endothelial cell plasticity. *Nat. Commun.* **8**, 14361 (2017).
15. Thambyrajah, R. et al. New insights into the regulation by RUNX1 and GFI1(s) proteins of the endothelial to hematopoietic transition generating primordial hematopoietic cells. *Cell Cycle* **15**, 2108–2114 (2016).
16. Blaser, B. W. & Zon, L. I. Making HSCs in vitro: don't forget the hemogenic endothelium. *Blood* **132**, 1372–1378 (2018).
17. Ottersbach, K. Endothelial-to-haematopoietic transition: an update on the process of making blood. *Biochem. Soc. Trans.* **47**, 591–601 (2019).
18. Dzierzak, E. & Bigas, A. Blood development: hematopoietic stem cell dependence and independence. *Cell Stem Cell* **22**, 639–651 (2018).
19. Pardanaud, L. et al. Two distinct endothelial lineages in ontogeny, one of them related to hemopoiesis. *Development* **122**, 1363–1371 (1996).
20. Pouget, C., Gautier, R., Teillet, M. A. & Jaffredo, T. Somite-derived cells replace ventral aortic hemangioblasts and provide aortic smooth muscle cells of the trunk. *Development* **133**, 1013–1022 (2006).
21. Yvernogeau, L., Auda-Boucher, G. & Fontaine-Perus, J. Limb bud colonization by somite-derived angioblasts is a crucial step for myoblast emigration. *Development* **139**, 277–287 (2012).
22. Ambler, C. A., Nowicki, J. L., Burke, A. C. & Bautch, V. L. Assembly of trunk and limb blood vessels involves extensive migration and vasculogenesis of somite-derived angioblasts. *Dev. Biol.* **234**, 352–364 (2001).
23. Christ, B., Huang, R. & Scaal, M. Amniote somite derivatives. *Dev. Dyn.* **236**, 2382–2396 (2007).
24. McGrew, M. J. et al. Efficient production of germline transgenic chickens using lentiviral vectors. *EMBO Rep.* **5**, 728–733 (2004).
25. McNagny, K. M. et al. Thrombomucin, a novel cell surface protein that defines thrombocytes and multipotent hematopoietic progenitors. *J. Cell Biol.* **138**, 1395–1407 (1997).
26. Thornton, M. A. & Poncz, M. Characterization of the murine platelet αIIb gene and encoded cDNA. *Blood* **94**, 3947–3950 (1999).
27. Yvernogeau, L. et al. An in vitro model of hemogenic endothelium commitment and hematopoietic production. *Development* **143**, 1302–1312 (2016).
28. Lassila, O., Eskola, J., Toivanen, P. & Dieterlen-Lievre, F. Lymphoid stem cells in the intraembryonic mesenchyme of the chicken. *Scand. J. Immunol.* **11**, 445–448 (1980).
29. Jaffredo, T., Gautier, R., Brajeul, V. & Dieterlen-Lièvre, F. Tracing the progeny of the aortic hemangioblast in the avian embryo. *Dev. Biol.* **224**, 204–214 (2000).
30. Taoudi, S. et al. Progressive divergence of definitive haematopoietic stem cells from the endothelial compartment does not depend on contact with the foetal liver. *Development* **132**, 4179–4191 (2005).
31. Muzumdar, M. D., Tasic, B., Miyamichi, K., Li, L. & Luo, L. A global double-fluorescent Cre reporter mouse. *Genesis* **45**, 593–605 (2007).
32. Sorensen, I., Adams, R. H. & Gossler, A. DLL1-mediated Notch activation regulates endothelial identity in mouse fetal arteries. *Blood* **113**, 5680–5688 (2009).
33. Oguro, H., Ding, L. & Morrison, S. J. SLAM family markers resolve functionally distinct subpopulations of hematopoietic stem cells and multipotent progenitors. *Cell Stem Cell* **13**, 102–116 (2013).
34. Kiel, M. J., Yilmaz, O. H., Iwashita, T., Terhorst, C. & Morrison, S. J. SLAM family receptors distinguish hematopoietic stem and progenitor cells and reveal endothelial niches for stem cells. *Cell* **121**, 1109–1121 (2005).
35. Langfelder, P. & Horvath, S. WGCNA: an R package for weighted correlation network analysis. *BMC Bioinformatics* **9**, 559 (2008).
36. Richard, C. et al. Endothelio-mesenchymal interaction controls *runx1* expression and modulates the *notch* pathway to initiate aortic hematopoiesis. *Dev. Cell* **24**, 600–611 (2013).
37. Pardanaud, L. & Dieterlen-Lievre, F. Manipulation of the angiopoietic/hemangiopoietic commitment in the avian embryo. *Development* **126**, 617–627 (1999).

38. Noden, D. M. Embryonic origins and assembly of blood vessels. *Am. Rev. Respir. Dis.* **140**, 1097–1103 (1989).
39. Pudliszewski, M. & Pardanaud, L. Vasculogenesis and angiogenesis in the mouse embryo studied using quail/mouse chimeras. *Int. J. Dev. Biol.* **49**, 355–361 (2005).
40. Nguyen, P. D. et al. Haematopoietic stem cell induction by somite-derived endothelial cells controlled by *meox1*. *Nature* **512**, 314–318 (2014).
41. Qiu, J. et al. Embryonic hematopoiesis in vertebrate somites gives rise to definitive hematopoietic stem cells. *J. Mol. Cell Biol.* **8**, 288–301 (2016).
42. Palis, J. Hematopoietic stem cell-independent hematopoiesis: emergence of erythroid, megakaryocyte and myeloid potential in the mammalian embryo. *FEBS Lett.* **590**, 3965–3974 (2016).
43. Chen, M. J. et al. Erythroid/myeloid progenitors and hematopoietic stem cells originate from distinct populations of endothelial cells. *Cell Stem Cell* **9**, 541–552 (2011).
44. Christensen, J. L., Wright, D. E., Wagers, A. J. & Weissman, I. L. Circulation and chemotaxis of fetal hematopoietic stem cells. *PLoS Biol.* **2**, E75 (2004).
45. Beaudin, A. E. et al. A transient developmental hematopoietic stem cell gives rise to innate-like B and T cells. *Cell Stem Cell* **19**, 768–783 (2016).
46. Plein, A., Fantin, A., Denti, L., Pollard, J. W. & Ruhrberg, C. Erythro-myeloid progenitors contribute endothelial cells to blood vessels. *Nature* **562**, 223–228 (2018).
47. Chevallier, A., Kieny, M. & Mauger, A. Limb–somite relationship: origin of the limb musculature. *J. Embryol. Exp. Morphol.* **41**, 245–258 (1977).
48. Christ, B., Jacob, H. J. & Jacob, M. Experimental analysis of the origin of the wing musculature in avian embryos. *Anat. Embryol. (Berl)* **150**, 171–186 (1977).

Methods

Antibodies for immunohistochemistry and flow cytometry. Details of the antibodies are provided in Extended Data Table 2.

Grafts of avian PSM. WT and transgenic GFP chicken (*Gallus gallus*) eggs were incubated at 38 ± 1 °C in a humidified atmosphere until embryos reached the appropriate stage established using Hamburger and Hamilton development tables[49]. GFP chickens were generated and provided by the Roslin Institute[24]. An artificial dark field was obtained by injecting Indian ink, diluted 1:1 in PBS, beneath the host embryos. Microsurgery was performed on the right side of the host. The PSM attached to the last formed somite was removed over a length corresponding to 5–10 somites. PSMs were rinsed in DMEM (PAA Laboratories)/10% fetal calf serum (FCS, Eurobio) and transplanted into a host submitted to the same ablation. Grafts were performed according to the original dorso-ventral and antero–posterior orientations. The chimaeric embryos were incubated and analysed at several time points, as shown in Extended Data Table 1.

After hatching, PSM grafted chickens were housed at the Gemeenschappelijk Dierenlaboratorium facility until they reached adulthood. Animals were housed according to institutional guidelines, and procedures were performed in compliance with Standards for Care and Use of Laboratory Animals, with approval from the Dutch Animal Experiment Committee.

Chicken cell staining and analysis. Chicken BM cells were flushed with PBS containing 5% FCS (Gibco; PBS/FCS). The suspension was washed and passed through successive gauge needles (21, 23 and 26G, Terumo) to obtain a single-cell suspension. Thymus, spleen and bursa of Fabricius were crushed and the cell suspensions were filtered through a 40 µm nylon cell strainer (Falcon) and then washed twice in PBS/FCS.

Cell suspensions were then incubated with antibodies for 20 min on ice. Cells were washed and suspended in PBS supplemented with DAPI or 7-aminoactinomycin D (to exclude dead cells). Stained cells were analysed on a MACSQuant 10 (Miltenyi Biotec) or FACSCalibur (Becton Dickinson) system. Data were reanalysed using FlowJo 10.6.

Immunostainings on whole BM, thymus, thick embryo slices and PSM. BM and thymus were prepared as previously described in ref. [30]. Tissues were stained with anti-GFP, anti-CD45 and anti-MEP21 antibodies. A goat anti-rabbit IgG (H+L) coupled to Alexa Fluor 488, a goat anti-mouse IgG2a coupled to Alexa Fluor 555 and a goat anti-mouse IgG1 coupled to Alexa Fluor 647 (all from ThermoFisher Scientific) were used to reveal the anti-GFP, anti-CD45 and anti-MEP21 antibodies, respectively. Thick slices and dissected PSM were stained with anti-CD45 and anti-MEP21 antibodies. PSM was counterstained with DAPI. Transparent bone marrow, thymus, thick slices and PSM were imaged with a Zeiss LSM700 confocal microscope with a ×10 PlanApo dry objective. Three-dimensional reconstructions were generated from *z*-stacks with Imaris software ×64 9.3.1 and converted to QuickTime files (.mov).

Time-lapse confocal imaging of the chicken grafted BM. Transversal slices of E16 PSM grafted BMs were processed for time-lapse confocal imaging as described in refs. [8,50]. Briefly, E16-grafted BMs were gently flushed out of the bones. Transversal slices (200 µm thickness) of the marrow were obtained using a tissue chopper and stained with CD41-PE (clone 11C3, Bio-Rad) antibody for 20 min on ice. After three washes in PBS, slices were placed in a culture chamber, embedded in a 1% low-melting-point agarose gel. Overnight, five to six slices per experiment were sequentially time-lapse imaged (every 20 min) on a Zeiss LSM700 confocal microscope. The following day, slices were stained again with CD41-PE (clone 11C3, Bio-Rad) antibody, washed and imaged to assess the emergence of new HSPCs during the overnight imaging.

Mice. Animals were maintained at the Developmental Biology Laboratory animal facility accredited by the Direction Départementale de la Protection des Populations under no. C 75-05-13. Experiments were carried out in the same structure in accordance with the guidelines of the French Veterinary Department. Approval was obtained from the French Ministère de l'Enseignement Supérieur, de la Recherche et de l'Innovation under no. APAFIS #7865-2016120210295552 v4. ROSA26 mT/mG reporter mice contain a double-fluorescent Cre reporter that expresses membrane-targeted tandem dimer Tomato (mT) prior to Cre-mediated excision and membrane-targeted green fluorescent protein (mG) after excision[31]. ROSA26-stop-EYFP mutant mice have a *loxP*$^{-}$ flanked STOP sequence followed by the enhanced yellow fluorescent protein gene (EYFP) inserted into the *Gt(ROSA)26Sor* locus[51]. Pax3-Cre mice were generated by replacing the first Pax3-coding exon with a gene encoding Cre recombinase. Mice were grown as heterozygous[52]. The Tg(Cdh5Cre/ERT2) transgenic mouse line was generated by insertion of a tamoxifen-inducible Cre (CreERT2) into a large PAC clone of the *Cadh5* (VE-cadherin) gene, resulting in endothelium-specific expression[32].

Pax3-mTmG mice generation. Homozygous 6- to 12-week-old mT/mG females were mated with 8- to 20-week-old heterozygous Pax3-Cre males. Fetuses were collected between E19 and E21, phenotyped based on the GFP expression in the central nervous system, and analysed for their BM content.

Cdh5-YFP mice generation and induction. Homozygous 6- to 12-week-old ROSA-YFP females were mated with homozygous 8- to 20-week-old Tg(Cdh5-Cre/ERT2) males. After birth, inductions were made in 50/50 male:female ratio animals by intra-peritoneal injections of tamoxifen (T5648, Sigma) diluted in corn oil (C8267, Sigma).

Mouse BM analysis and cell sorting. Femurs and tibias were flushed with DMEM (Gibco) supplemented with 10% FCS (Eurobio). Cells were dissociated with collagenase type 1 (C0130, Sigma) 1.25 mg ml^{-1} in PBS + 10% FCS for 30 min at 37 °C, and washed twice with DMEM + 10% FCS. Between 1×10^6 and 5×10^6 cells were stained with fluorescent antibodies (Extended Data Table 2) in PBS + 0.5% BSA for at least 30 min at 4 °C. Cells were washed, and suspended in PBS + 0.5% BSA supplemented with 1.25 µg ml^{-1} DAPI (D9542, Sigma) for cell viability, and analysed on a MACSQuant VYB (Miltenyi Biotec) or a LSR II (Becton-Dickinson) flow cytometer. Data were reanalysed with FlowJo 10.6 software.

For cell sorting, after collagenase treatment and washing, red blood cells were lysed using Gey's solution for 5 min at 4 °C. After two washes with DMEM + 10% FCS, Lin depletion was performed by incubation of cells with purified Gr-1, Ter119, B220, CD11b, CD4 and CD8 antibodies in PBS + 0.5% BSA for 30 min at 4 °C. After washing, cells were incubated with goat anti-rat microbeads (Miltenyi Biotec) for 30 min at 4 °C. After washing, cells were applied to an LD column (Miltenyi Biotec) according to the manufacturer's guidelines and eluted Lin-cells were collected. Lin-cells were then stained with Sca1-PE and CD117(c-Kit)-PE-Cy7. LSK YFP$^+$ and YFP$^-$ cells were sorted using a FACS Aria III (Becton-Dickinson) cell sorter.

In vitro EHT testing. Ten to 15,000 144$^+$45$^-$ or 144$^+$45$^+$ sorted BM cells from six pooled eight-day-old mice were seeded on BioCoat collagen I 24 wells (Corning) in Optimem medium (Gibco) supplemented with 10% FCS (Hyclone), EGM2 SingleQuots (Lonza), 10 ng ml^{-1} mIL-3, 10 ng ml^{-1} mFLT3L, 20 ng ml^{-1} mSCF and 20 ng ml^{-1} mTPO. At day 4, floating cells were incubated with PE anti-mouse CD45 (Biolegend, Ozyme) and analysed on a MACSQuant 10 (Miltenyi Biotec) flow cytometer.

Analysis of transplantation capabilities. Adult C57BL/6-CD45.1 mice were exposed to a lethal single dose of 7.3 Gy (1.04 Gy min^{-1}) from an X-ray generator (320 kV, Philips). A total of 2,000 sorted LSK YFP$^+$ or YFP$^-$ cells from Cdh5-YFP mice (genetic background C57BL/6-CD45.2) were co-injected intravenously into the retro-orbital venous plexus with 2×10^5 normal C57BL/6-CD45.1 BM cells. Peripheral blood was collected at 2, 3, 4, 7 and 11 weeks after engraftment and nucleated cells were incubated with allophycocyanin (APC) anti-mouse CD45.1, and PE anti-mouse CD45.2 (Biolegend, Ozyme), and analysed by flow cytometry for the presence of donor-derived (CD45.2$^+$) cells. Mice were euthanized at 14 weeks and BMs were analysed for grafting potential.

Transcriptomic analysis. Sorted LSK YFP$^+$ and YFP$^-$ cells were lysed with 350 µl RLT+ buffer (RNeasy Plus Micro kit, Qiagen) and stored at −80 °C. All RNA isolations were performed at the same time, according to the manufacturer's guidelines. Affymetrix mouse gene 1.0 (HC AGM, CD144$^+$CD45$^+$ AGM, EC AGM) or 2.0 ST arrays (LSK YFP$^+$, LSK YFP$^-$, HC BM, LSK CD150$^+$ BM cells) were used. RNA concentration and integrity were evaluated with the Agilent Bioanalyzer 2100 (Genom'IC Facility platform, Cochin Institute). To correct for probe set definition inaccuracy, we used version 17 of the custom chip definition file (CDF).

Design of the screening strategy and microarray analysis. Non-supervised analyses were performed on the global transcriptome of six samples (three YFP$^+$ and three YFP$^-$ replicates) and data were represented with PCA. Genes upregulated in YFP$^+$ versus YFP$^-$ cells were selected using ANOVA. Selected gene sets were then processed using the Database for Annotation, Visualization and Integrated Discovery (DAVID) (http://david.ncifcrf.gov)[53,54] to identify representative biological activities of YFP$^+$ versus YFP$^-$ LSKs.

For PCA, hierarchical clustering and other statistical analyses, we used Partek and JMP software. To find how our neonate BM samples were positioned in relation to E11.5 AGM and three-week-old BM samples, we merged the present data with previously generated AGM and adult BM transcriptomes. The AGM samples consisted of cells sorted according to the expression of CD144 (CDH5), CD34, CD45 (PTPRC) and c-Kit (CD117), enabling us to discriminate immature HCs, broadly equivalent to HSC (CD144^{med}CD45$^+$ or CD34$^+$c-Kit$^+$), from mature HCs (CD144^{med}CD45$^+$ or CD34^{med}c-Kit^{med}), and ECs (CD144$^+$CD45$^-$). The BM samples consisted of cells sorted according to the expression of CD150 (SLAMF1), c-Kit, Sca-1 and markers of the different haematopoietic lineages (Lin), enabling us to discriminate immature HCs, broadly equivalent to HSC (CD150$^+$c-Kit$^+$Sca-1$^+$Lin$^-$), from mature HCs (Lin$^+$). A new matrix was therefore generated corresponding to 28 samples and including 18,920 genes. After removal of the batch effect using Partek (three different experiments were merged, all the samples were biological triplicates except for the BM samples, where quadruplicates were used), PCA was carried out. ANOVA was then performed comparing YFP$^+$ versus YFP$^-$ cells with $P < 0.001$, resulting in 2,479 DEGs, 1,123 upregulated and 1,356

downregulated. Because YFP$^+$ cells were clearly discriminated from YFP$^-$ cells on the PC1-versus-PC2 score plot of the PCA, we resorted to WGCNA[35] to unravel the different gene networks using the contrast between the YFP$^+$ and YFP$^-$ populations as the trait. The selected parameters for analysis were as follows: power, 26; adjacency, signed; correlation, Pearson's; linkage, average; minimum module size, 30. For the Cytoscape connectivity, plot edges were selected above a given weight (intramodular topological overlap measure) threshold. Graph layout was force-directed.

Statistics and reproducibility. All of the data points are biological replicates that were randomly assigned without investigator blinding. All experiments were replicated at least three times. All the images are representative of at least three independent biological samples. No data were excluded. Statistical significance was determined using Microsoft Excel or GraphPad Prism5 Software. Bar charts and plots in Figs. 2j–l, 4c–e, 5d and 6e and Extended Data Figs. 4a,c, 6a,c, 7c,d and 8e represent means ± s.e.m. Comparisons were performed by two-tailed, unpaired Student's *t*-tests. The number of experimental repeats are indicated in the figure legends. Significance was taken as $P < 0.05$ with a confidence interval of 95%: $^*P < 0.05$; $^{**}P < 0.01$; $^{***}P < 0.001$; $^{****}P < 0.0001$.

Reporting Summary. Further information on research design is available in the Nature Research Reporting Summary linked to this article.

Data availability

Microarray data that support the findings of this study have been deposited in the Gene Expression Omnibus (GEO) under accession codes GSE122857, GSE133804 and GSE133812. All other data supporting the findings of this study are available from the corresponding author on reasonable request.

References

49. Hamburger, V. & Hamilton, H. L. A series of normal stages in the development of the chick embryo. *J. Morphol.* **88**, 49–92 (1951).
50. Boisset, J. C., Andrieu-Soler, C., van Cappellen, W. A., Clapes, T. & Robin, C. Ex vivo time-lapse confocal imaging of the mouse embryo aorta. *Nat. Protoc.* **6**, 1792–1805 (2011).
51. Srinivas, S. et al. Cre reporter strains produced by targeted insertion of EYFP and ECFP into the ROSA26 locus. *BMC Dev. Biol.* **1**, 4 (2001).
52. Engleka, K. A. et al. Insertion of Cre into the *Pax3* locus creates a new allele of *splotch* and identifies unexpected *Pax3* derivatives. *Dev. Biol.* **280**, 396–406 (2005).
53. Huang, D. W., Sherman, B. T. & Lempicki, R. A. Systematic and integrative analysis of large gene lists using DAVID bioinformatics resources. *Nat. Protoc.* **4**, 44–57 (2009).
54. Huang, D. W. et al. Extracting biological meaning from large gene lists with DAVID. *Curr. Protoc. Bioinformatics* **13**, 13.11 (2009).

Acknowledgements

We apologize to those investigators whose important work we were unable to cite or describe due to space constraints. We thank D. Traver for critical reading of the manuscript and S. Gournet for help in image preparation. We are indebted to R. Adams for his sharing of the Tg(Cdh5Cre/ERT2) transgenic mouse line and to S. Germain for providing us with the founders. We thank the Cell Imaging and Flow Cytometry facility of the IBPS (Paris, France) for access and technical support in confocal image acquisition and the Genom'IC platform at Cochin Institute, Paris for their invaluable help with transcriptomic samples treatment. This work was supported by CNRS, UPMC, Fondation Les Treilles (L.Y.), an EMBO short-term fellowship (L.Y.), MERI and FRM PhD fellowships (H.K.) and grants from FRM (DEQ20100318258) and an ANR/CIRM joint grant (ANR/CIRM 0001–02) in T.J.'s laboratory. The production of the GFP$^+$ chicken embryos was supported by grants from BBSRC and the Wellcome Trust. Part of the work and L.Y. were supported by a European Research Council grant (ERC, project no. 220-H75001EU/HSCOrigin-309361) and a TOP subsidy from NWO/ZonMw (912.15.017) in C.R.'s laboratory.

Author contributions

L.Y. and T.J. conceived the project. L.Y. and T.J. designed the experiments on chicken embryos, performed chicken somite grafts and interpreted data. L.Y. performed chicken grafts, carried out immunohistological analysis and performed FACS analysis. R.G. performed chicken graft analysis. L.P. performed all mouse work, including transplantation studies, and analysed the data. H.S. provided GFP transgenic chickens. V.R. and F.R. provided the Pax3CRE X Rosa mTmG mice and critical associated materials. H.K. analysed the YFP$^+$ transcriptome versus the YFP$^-$ transcriptome. P.C. analysed transcriptomes, performed network analyses and interpreted data. M.S. designed Pax3CRE X ROSAmTmG and the initial VECAD-Cre ERT X Rosa 26 approaches, analysed the data and provided the additional mouse embryonic and BM adult transcriptomes. C.R. and L.Y. designed and supervised the experiments on adult chickens and the live imaging on sections. T.J. wrote the manuscript. L.Y. and C.R. provided significant input for data analyses, findings, interpretations and manuscript writing.

Competing interests

The authors declare no competing interests.

Additional information

Extended data is available for this paper at https://doi.org/10.1038/s41556-019-0410-6.

Supplementary information is available for this paper at https://doi.org/10.1038/s41556-019-0410-6.

Correspondence and requests for materials should be addressed to T.J.

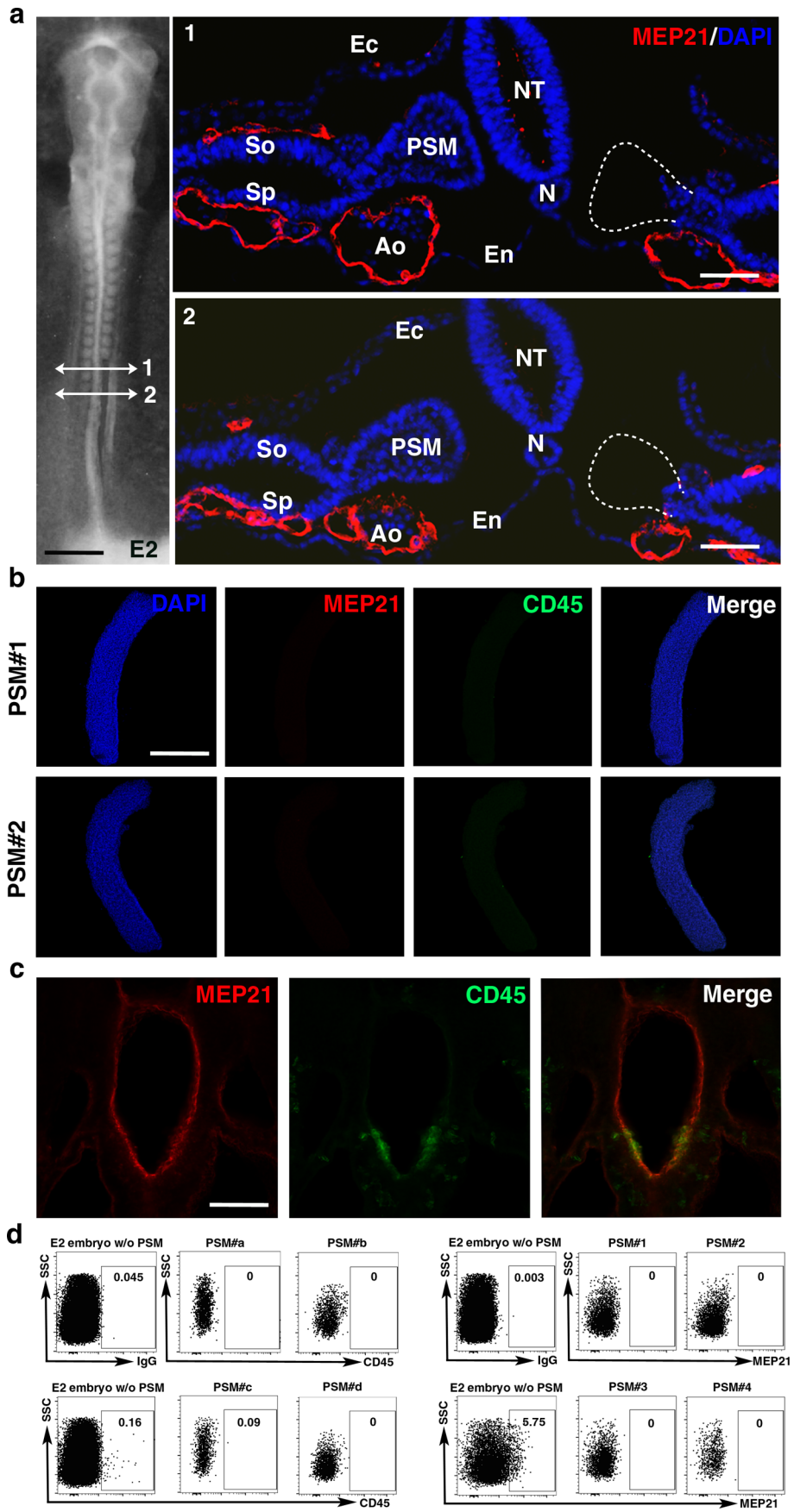

Extended Data Fig. 1 | See caption on next page.

Extended Data Fig. 1 | PSM removal experiment. a, E2 (15-somite stage, HH11/12) wild-type chicken embryo submitted to a PSM ablation. White arrows located the regions of transverse histological analysis at two representative anterior and posterior levels displayed in 1 and 2. MEP21 (red) and DAPI (blue) staining showed that only the PSM was removed without disturbing the surrounding tissues (10 chicken embryos). **b**, Whole mounts of two PSMs isolated from six E2 (15-somite stage, HH11/12) wild-type embryos and stained with DAPI (blue), MEP21 (red) and CD45 (green) antibodies, showing that PSMs do not contain any ECs or HCs after dissection. Two independent examples are shown (#1, #2) (6 chicken embryos). **c**, Mid trunk, thick transverse section of an E3 chicken embryo stained with MEP21 (red) and CD45 (green) antibodies shown as positive control of the immunostainings. Of note, PSMs (**b**) and thick slice (**c**) were stained at the same time, using the same antibody solutions. **d**, Representative FACS analysis on single PSMs isolated from 8 independent 13-15 somite stage embryos showing no contamination by haematopoietic (CD45) or endothelial (MEP21) cells. Controls are two whole embryos without PSMs showing the presence of $CD45^+$ haematopoietic and $MEP21^+$ endothelial cells. Ao, Aorta; Ec, Ectoderm; En, Endoderm; Nc, Notochord; NT, Neural Tube; PSM, Presomitic mesoderm; So, Somatopleura; Sp, Splanchnopleura. Scale bars, 200μm in **a**, 25μm in **a**1**, a**2; 50μm in **b** and **c**.

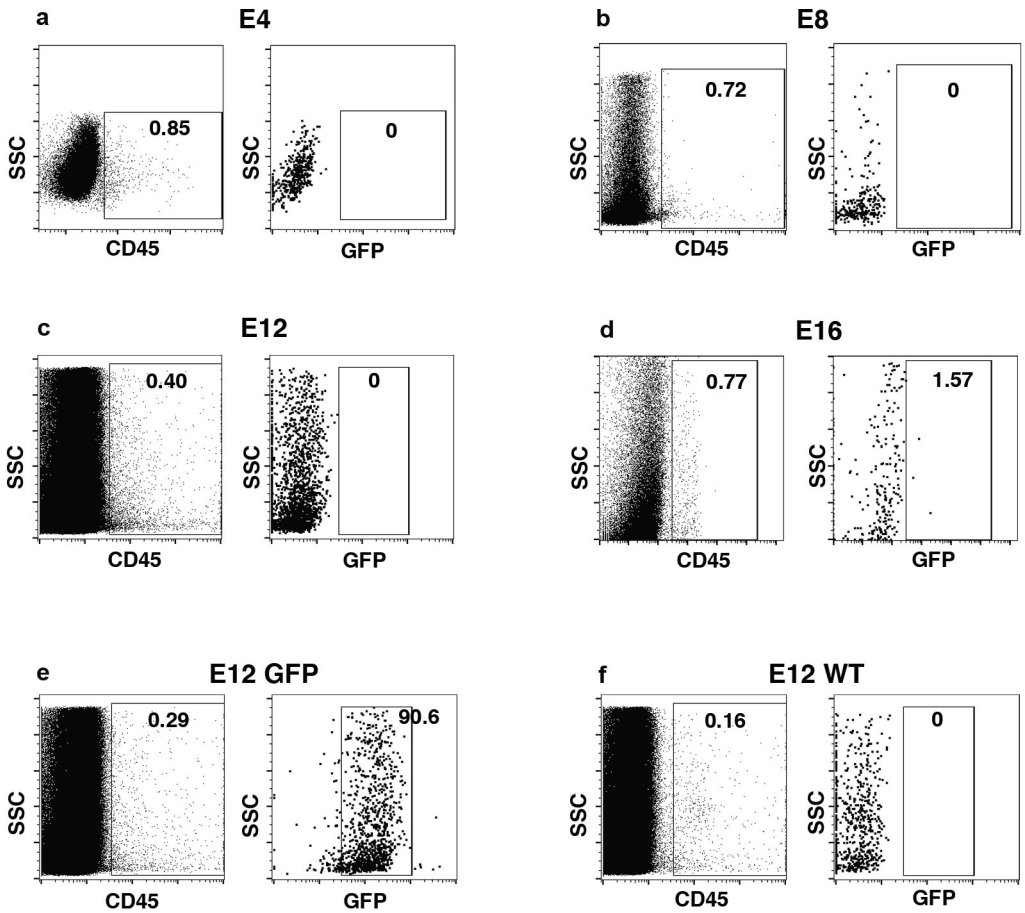

Extended Data Fig. 2 | GFP⁺CD45⁺ haematopoietic cells in circulating blood of the grafted or control embryos with age. a-f, CD45 expression in the sample (left) and GFP plot in the CD45⁺ population (right). **a-d**, chimeric embryos. **a**, E4 embryo. **b**, E8 embryo. **c**, E12 embryo. **d**, E16 embryo. Of note, only E16 embryos show GFP⁺ cells within the CD45⁺ fraction. **e**, E12 GFP transgenic embryo. **f**, E12 WT embryo. 23 chicken embryos analysed. See Extended Data Table 1 for details. Data representative of 4 independent experiments.

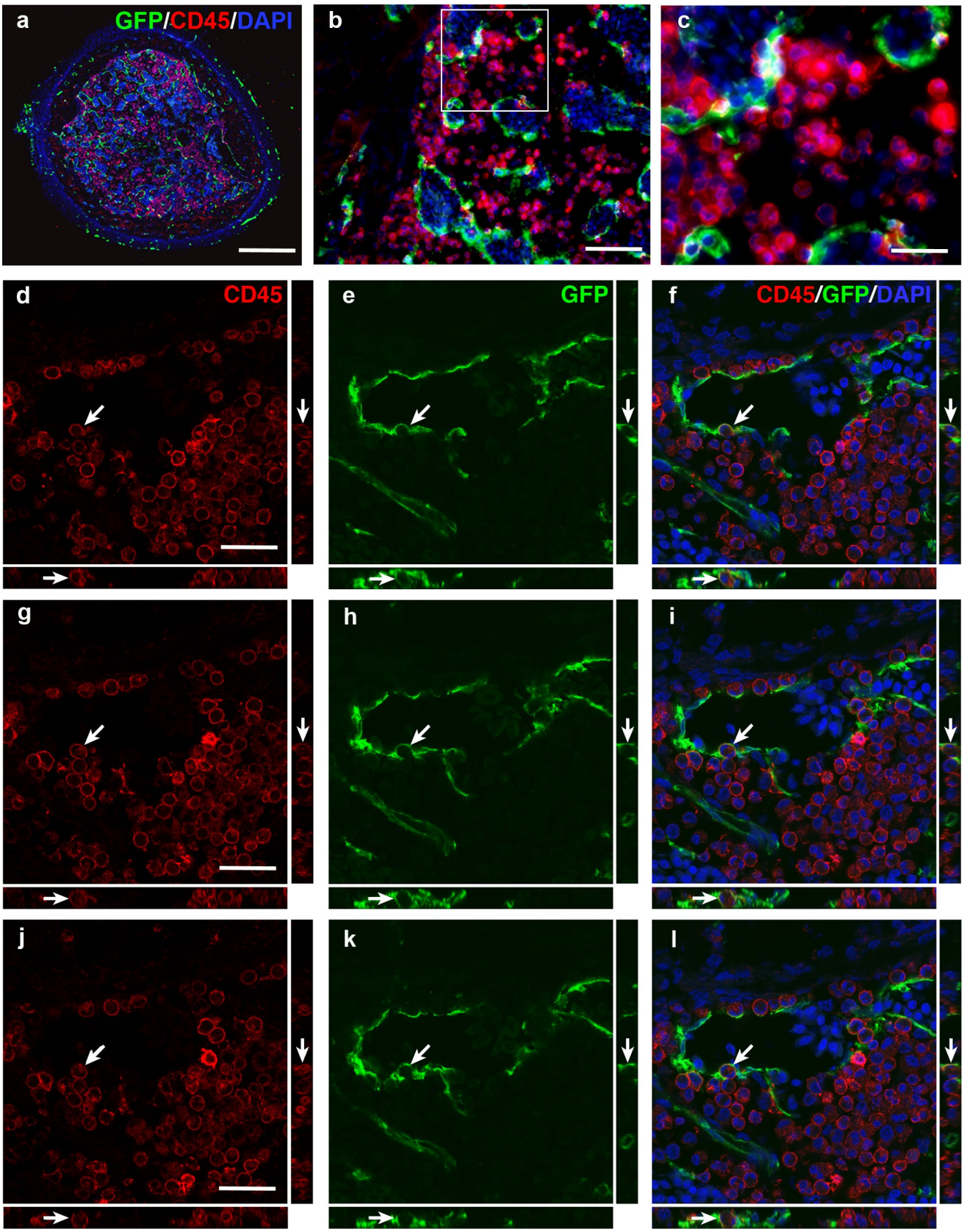

Extended Data Fig. 3 | GFP⁺ somite-derived cells contribute to E16/E17 bone marrow CD45⁺ haematopoietic production. a-c, Representative fluorescent cross section of the limb bone showing the co-distribution of GFP⁺ sinusoid cells and CD45⁺ cells. **b**, Enlargement of the bone marrow showing GFP⁺CD45⁺ cells lining the sinusoids. **c**, Enlargement of the frame in **b**, showing the double positive cells. **d-l**, Series of confocal cross sections separated by 1µm, showing a GFP⁺CD45⁺ cell (white arrow). **d, g, j**, CD45 staining. **e, h, k**, GFP signal. **f, i, l**, Merged CD45, GFP and DAPI. Right and bottom banners correspond to YZ and XZ projections of the confocal image, respectively. Experiments were repeated 16 times with similar results (see Extended Data Table 1 for details). Confocal analysis was performed 5 times with similar results. Scale bars in **a**, 200µm; in **b**, 40µm; in **c**, 15µm; in **d-l**, 20µm.

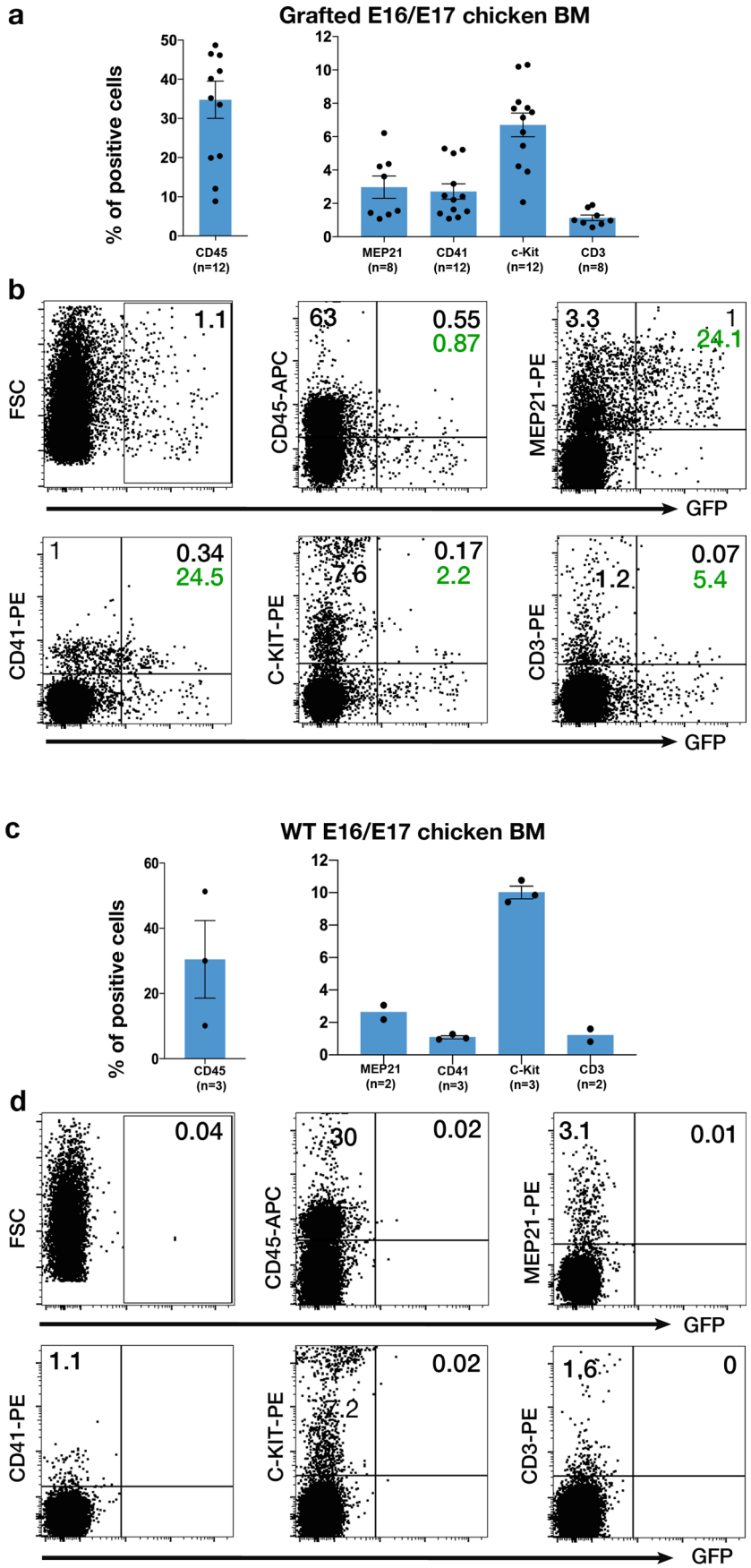

Extended Data Fig. 4 | See caption on next page.

Extended Data Fig. 4 | Flow cytometry analysis reveals the presence of endothelial and haematopoietic cells expressing GFP in the E16-grafted chicken BM. Distribution of CD45, MEP21, CD41, c-KIT, and CD3 populations in grafted (**a, b**) or wild-type (**c**, **d**) BM mononucleated cells. **a**, n = 12 independently grafted animals were used for CD45, CD41, c-KIT and CD3 expression and n = 8 for MEP21. **b**, Representative flow cytometry analysis of an E16/E17 grafted BM showing that GFP^+ cells derived from the PSM graft contributed to all lineages. Numbers in green indicate the percentage of GFP^+ cells in each population (that is in $CD45^+$, $MEP21^+$, $CD41^+$, c-KIT^+ and $CD3^+$ populations). **c**, n = 3 independent WT animals were used for CD45, CD41, c-KIT expression analysis, n = 2 animals were used for MEP21 and CD3 expression analysis. **d**, Representative flow cytometry analysis of an E16/E17 WT BM. Data in **b** representative of 4 independent experiments, 3 in **d**. Error bars are mean ± SEM.

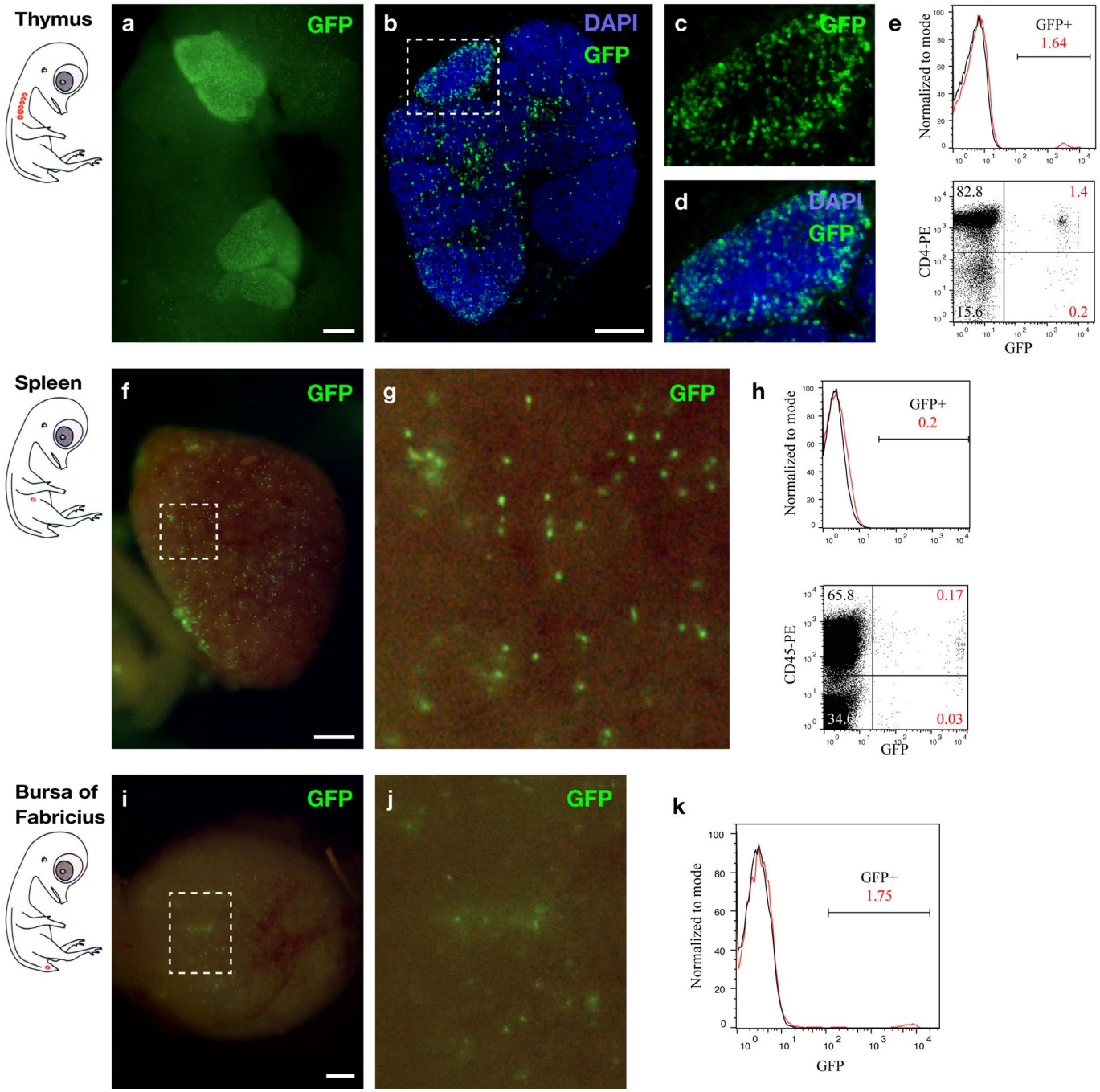

Extended Data Fig. 5 | PSM-derived cells provide haematopoietic precursors able to colonize the secondary haematopoietic organs of E16/E17 grafted chickens. a, **f**, **i**, Global views of the thymus (**a**), spleen (**f**) and bursa of Fabricius (**i**) of an E16 chicken colonized by GFP$^+$ PSM-derived grafted cells. **a**, Most of the thymus lobes were colonized by GFP$^+$ cells (3 chickens). **b**, Immunostaining (with DAPI) of a thymus transverse section. **c-d**, Higher magnification of the frame in (**b**). GFP (**c**) and merge of DAPI and GFP (**d**). **e**, Flow cytometry analysis of an E16/E17 thymus (2 chickens) revealed the contribution of GFP$^+$ PSM-derived cells to the whole thymus and more precisely to the T lineage (GFP$^+$CD4$^+$). **g**, Higher magnification of the frame in (**f**), showing dispersed GFP$^+$ cells in the spleen (2 chickens). **h**, Flow cytometry analysis of the spleen, showing the contribution of GFP$^+$ PSM-derived cells to the whole spleen and more precisely to the CD45$^+$ haematopoietic lineage (2 chickens). **j**, Higher magnification of the frame in (**i**) showing dispersed GFP$^+$ cells in the bursa (2 chickens). **k**, Flow cytometry analysis showing that the bursa of Fabricius, located far away from the PSM graft, was also colonized by PSM-derived haematopoietic progenitors that derived from the graft (2 chickens). Drawings are shown on the left side of the organ pictures to locate the thymus, spleen and bursa of Fabricius in an E16/E17 chicken. Scale bars in **a**, **b**, **f**, **i**: 100µm.

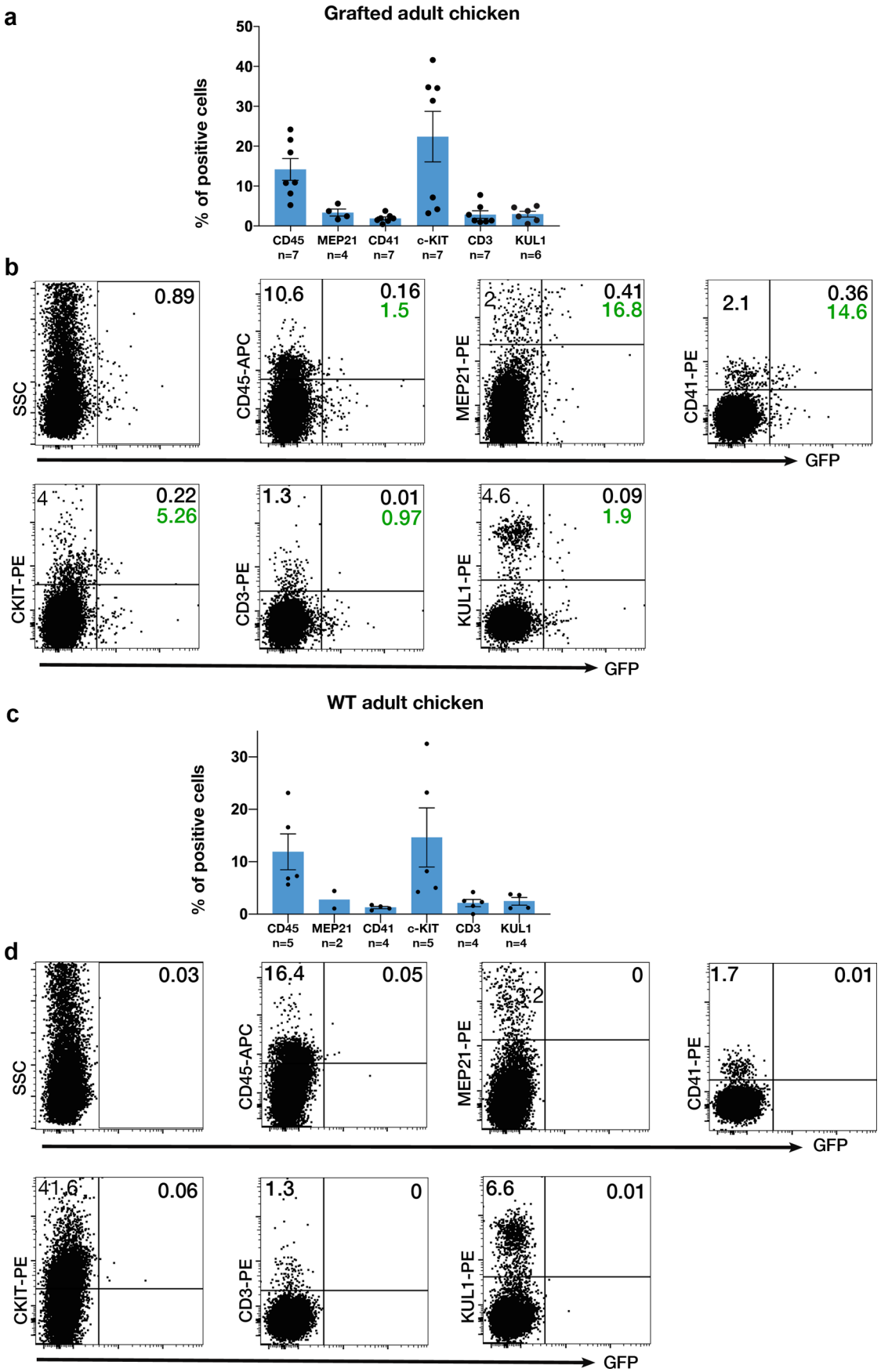

Extended Data Fig. 6 | See caption on next page.

Extended Data Fig. 6 | Flow cytometry analysis reveals the presence of endothelial and haematopoietic cells expressing GFP in adult BM grafted chickens. Distribution of CD45, MEP21, CD41, c-KIT, CD3 and KUL1 populations in grafted (**a, b**) and wild-type (**c, d**) adult BM mononucleated cells. **a**, Grafted chickens. CD45 (n = 7), MEP21 (n = 4), CD41 (n = 7), c-KIT (n = 7), CD3 (n = 7) and KUL1 (n = 6) independent chickens were used for the analysis. **b**, Representative multilineage flow cytometry analysis of a grafted adult BM showing that GFP^+ cells derived from the PSM graft contributed to all lineages. Numbers in green indicate the percentages of GFP^+ cells in each population (that is in $CD45^+$, $MEP21^+$, $CD41^+$, $c\text{-}KIT^+$, $CD3^+$ and $KUL1^+$ populations). **c**, Wild-type animals. CD45 (n = 5), CD41 (n = 4), c-KIT (n = 5), CD3 (n = 4) and KUL1 (n = 4); independent animals were used for the analysis. n = 2 animals were used for MEP21 expression analysis. **d**, Representative multilineage flow cytometry analysis of a wild-type adult BM showing the absence of GFP staining. Error bars represent mean ± SEM. Data in **b** and **d** representative of 4 independent experiments.

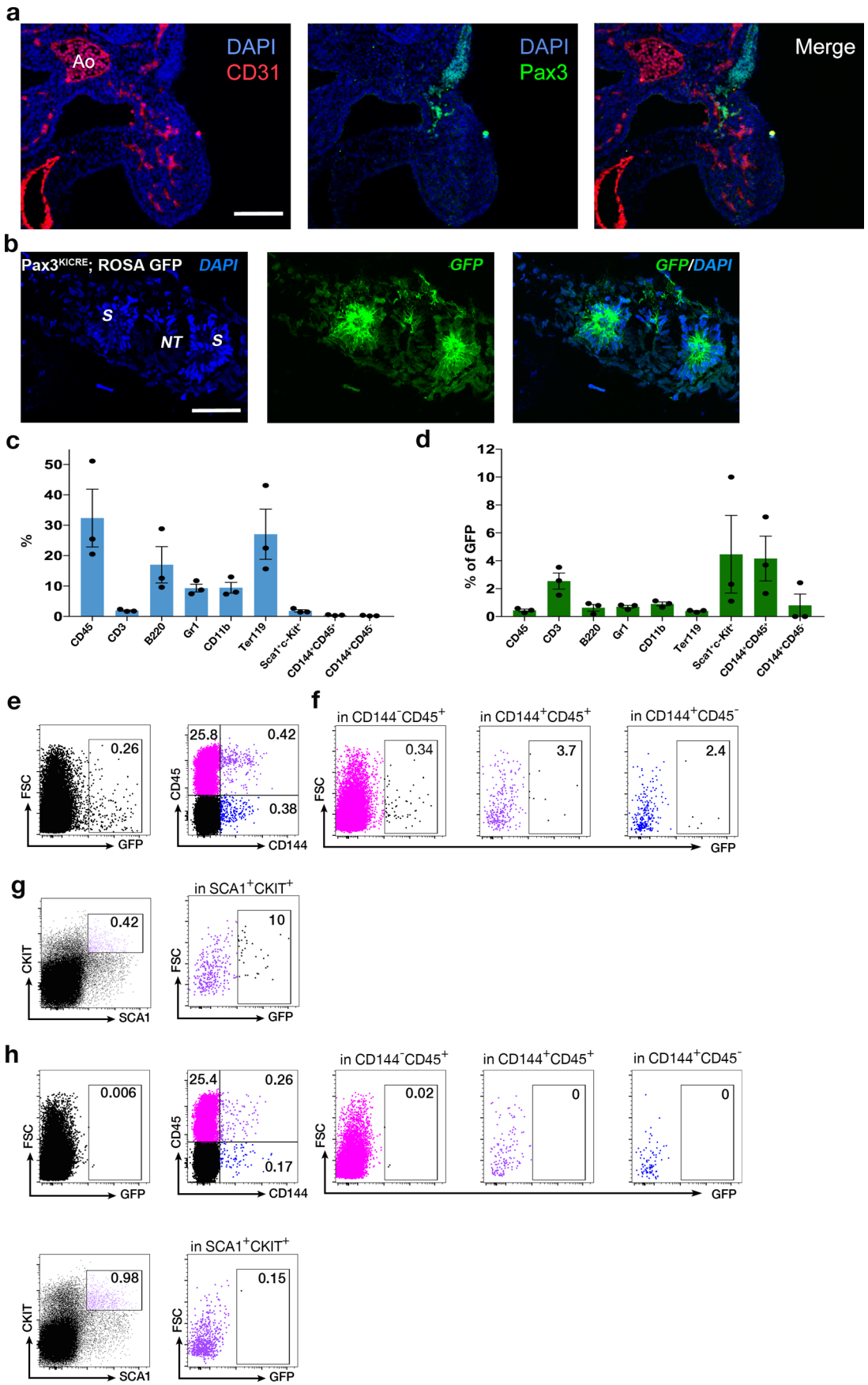

Extended Data Fig. 7 | See caption on next page.

Extended Data Fig. 7 | Pax3^{+} somite-derived cells do not contribute to the aorta haematopoieisis but contribute to the endothelial and haematopoietic lineages in the late fetal BM. a, Transverse section through the aorta of an E10.5 Pax3 GFP^{+} mouse embryo at the mid-trunk level. CD31 (red, left), Pax3-GFP (green, middle) double staining counterstained with DAPI (blue). Right panel represents the merge (5 mice). **b**, Cross section of a Pax3^{KICRE}; ROSA GFP embryo at E8.5 showing that this model tags the somite and recapitulates the Pax3 GFP expression at the same stage (5 mice). **c**, Flow cytometry analysis of the endothelial and haematopoietic lineages in the BM of Pax3-Cre/mTmG fetuses at E19-E21. n = 3 fetuses from 3 independent experiments. **d**, Flow cytometry analysis showing GFP^{+} cell (that is somite-derived cell) contribution to the different endothelial and haematopoietic populations. Mouse somite-derived cells mostly contributed to fetal/new-born BM CD3^{+}, Sca1^{+}c-Kit^{+} and CD144^{+}CD45^{+} cell populations. n = 3 foetuses from 3 independent experiments. **e**, Representative GFP expression in mononucleated BM cells. **f**, Representative flow cytometry analysis of the mononucleated BM cells revealed GFP^{+} cells mainly in the CD144^{+}CD45^{+} population. **g**, Flow cytometry analysis showing the presence of GFP^{+} cells in the Sca1^{+}c-KIT^{+} population (that is HSPC population). **h**, Negative controls are non-recombined fetuses. Data represent mean ± SEM. Data in **e**-**h** representative of 2 independent experiments. Scale bars 350μm in **a**; 200μm in **b**.

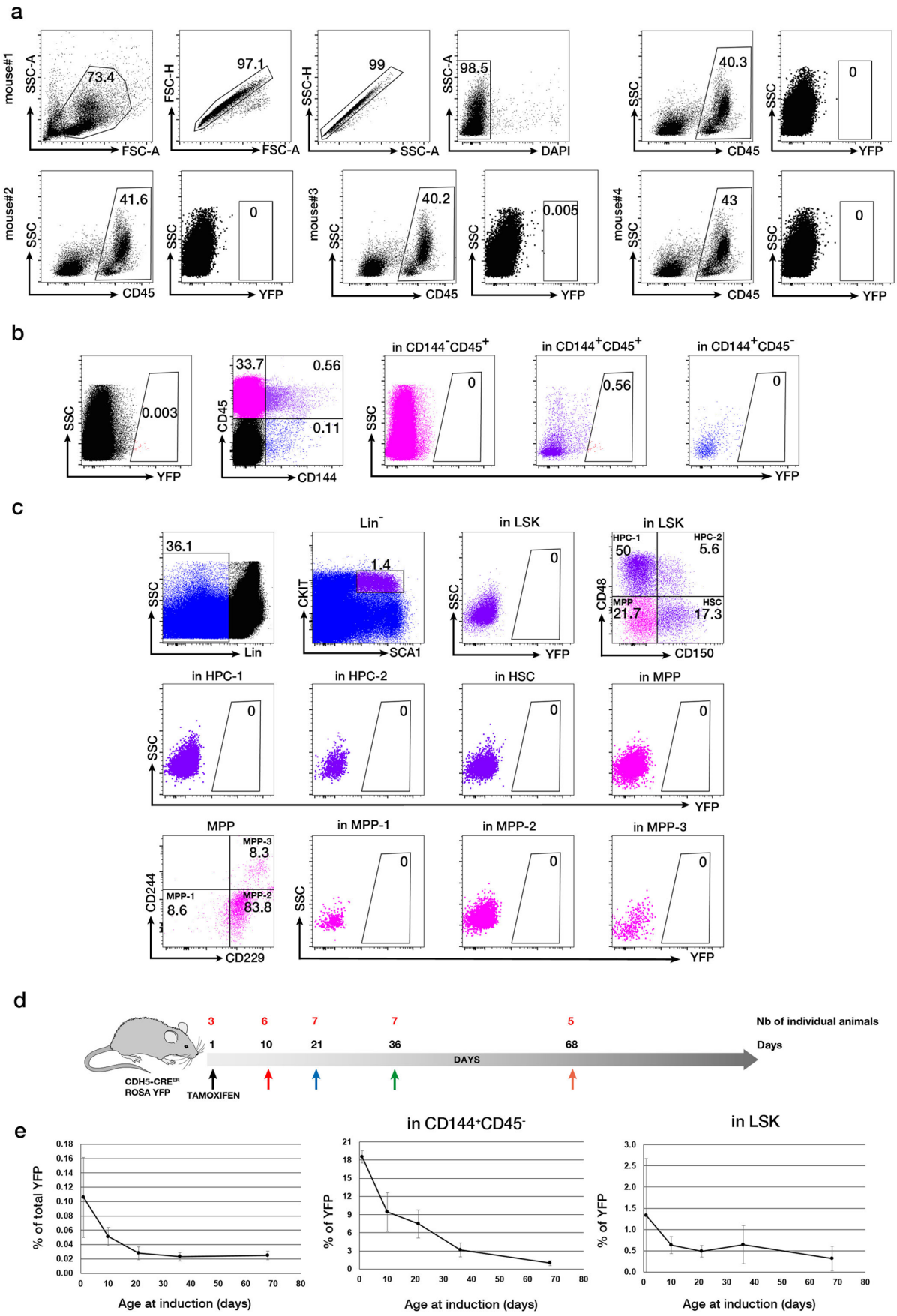

Extended Data Fig. 8 | See caption on next page.

Extended Data Fig. 8 | YFP expression on negative controls and YFP tracing following induction in VE-cadherin$^+$ cells at different time points after birth. **a**, Flow cytometry analysis for the presence of YFP$^+$ cells in the CD45$^+$ fraction of the BM immediately after the last tamoxifen injection. Representative new-born mice injected with tamoxifen at post-natal days 1, 2, and 3 and analysed for the expression of CD45 and YFP at day 4. No CD45$^+$ YFP$^+$ cells were found indicating the absence of contamination by haematopoietic progenitors expressing VE-Cadherin (11 animals in 3 independent experiments). The gating strategy is shown for mouse #1. **b, c**, BM from a representative non-induced mouse at 27 post-natal days. **b**, Representative flow cytometry analysis showing the absence of YFP expression in mononucleated BM cells and in the CD144$^-$CD45$^+$, CD144$^+$CD45$^+$ and CD144$^+$CD45$^-$ cell fractions (4 animals in 2 independent experiments). **c**, Representative flow cytometry analysis of the mononucleated BM cells showing the absence of YFP expression in the Sca1$^+$c-KIT$^+$ population (that is HSPC population) and in the different HSC, HPC and MPP populations (2 independent experiments). **d**, Scheme showing the activation of YFP in VE-Cadherin$^+$ (CDH5) cells by tamoxifen injection at different time points after birth (coloured arrows). **e**, Analysis of the percentages of total YFP$^+$ cells, and YFP$^+$ cells in CD144$^+$CD45$^-$ and LSK populations at 21 days post tamoxifen injection. Of note, the x axis values represent the age of the mice from the time of tamoxifen injection. n = 3 mice for d1, n = 6 for d10, n = 7 for d21, n = 7 for d36, n = 5 for d68. Error bars are mean ± SEM. Data in **a**-**c** representative of 2 independent experiments.

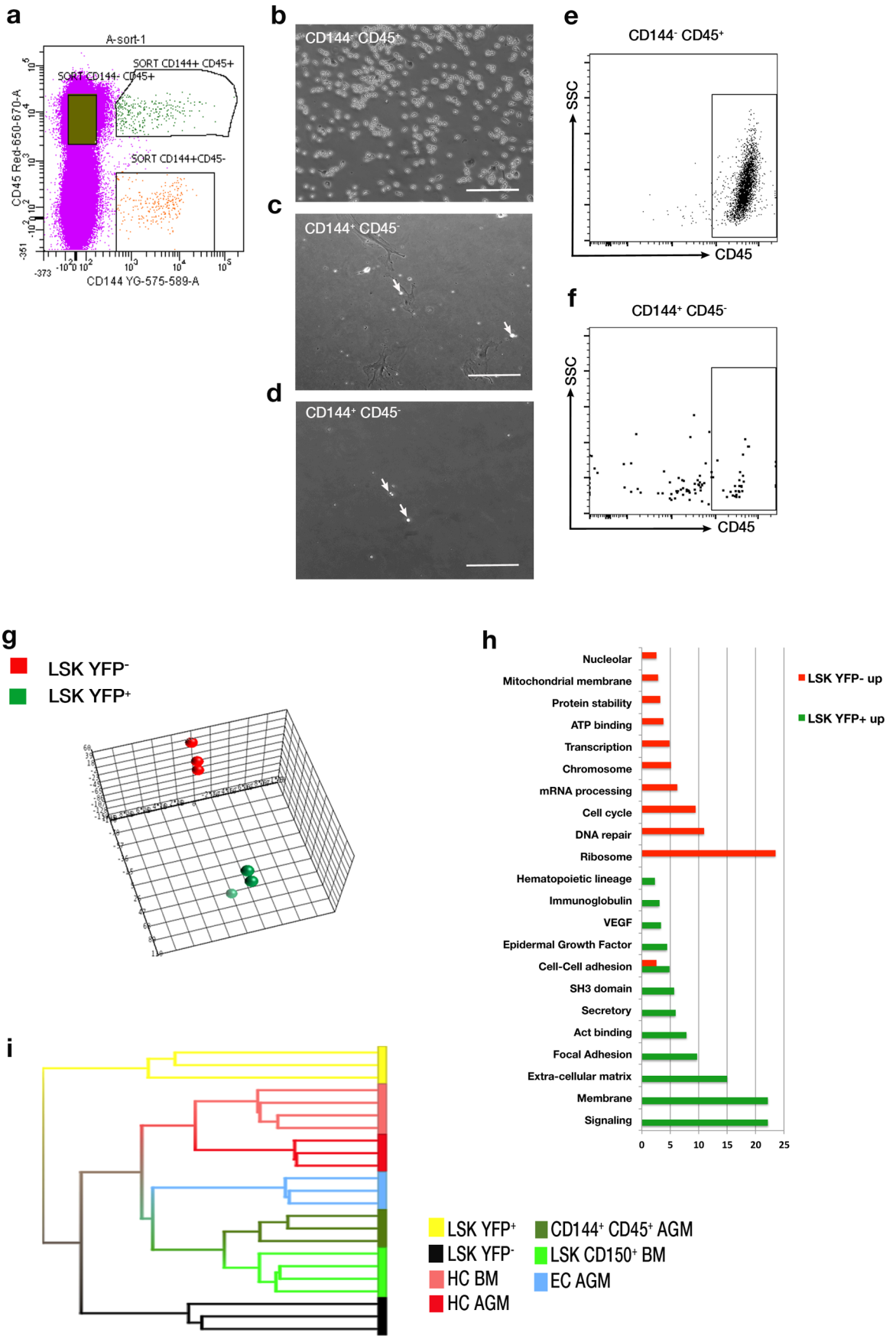

Extended Data Fig. 9 | See caption on next page.

Extended Data Fig. 9 | Haemogenic potential of BM ECs and transcriptome characterisation of the YFP$^+$ and YFP$^-$ LSK cells. a, representative flow cytometry profile showing the gates used to isolate the CD144$^+$CD45$^-$ and the CD144$^-$CD45$^+$ populations. Image representative of 7 mice. **b**-**e**, representative pictures of the CD144$^-$CD45$^+$ (**b**) and CD144$^+$CD45$^-$ (**c**, **d**) cells from 8-day old mouse bone marrow in culture in the endothelial/haematopoietic medium. A high number of floating cells are present in the CD144$^-$CD45$^+$ cells fraction (**b**). Flat adherent cells (in **c**) and round, floating, haematopoietic-like cells (arrows in **c** and **d**) are present in the CD144$^+$CD45$^-$ cell fraction after 4 days of culture. Image representative of 3 experiments. Bar = 10μm. **e**, **f**, representative FACS analysis of the CD45$^+$ populations generated after 4 days of culture from the CD144$^-$CD45$^+$ (**e**) and the CD144$^+$CD45$^-$ (**f**) cell populations. Image representative of 3 experiments. **g**, PCA with the entire set of mRNAs (30,922 genes) as variables and the basic set of YFP$^+$ (green) and YFP$^-$ (red) LSK cells as observations. The two types of transcriptomes were strongly separated (3 biological replicates per population). **h**, Major GO categories given by DAVID for the gene sets up-regulated in YFP$^+$ (green) and YFP$^-$ (red) LSK cells. **i**, Hierarchical clustering obtained with the 23 samples (3 biological replicates per population except for HC BM and LSK CD150$^+$ BM where quadruplicates were used) as observations and the gene set of 2056 DEGs (986 up, 1070 down) as variables was generated from the PCA displayed in Fig. 6a, bottom panel. Branch organisation reflects the association between the different samples displayed on the PCA. Scale Bars: 50μm in **b**, **c**, **d**.

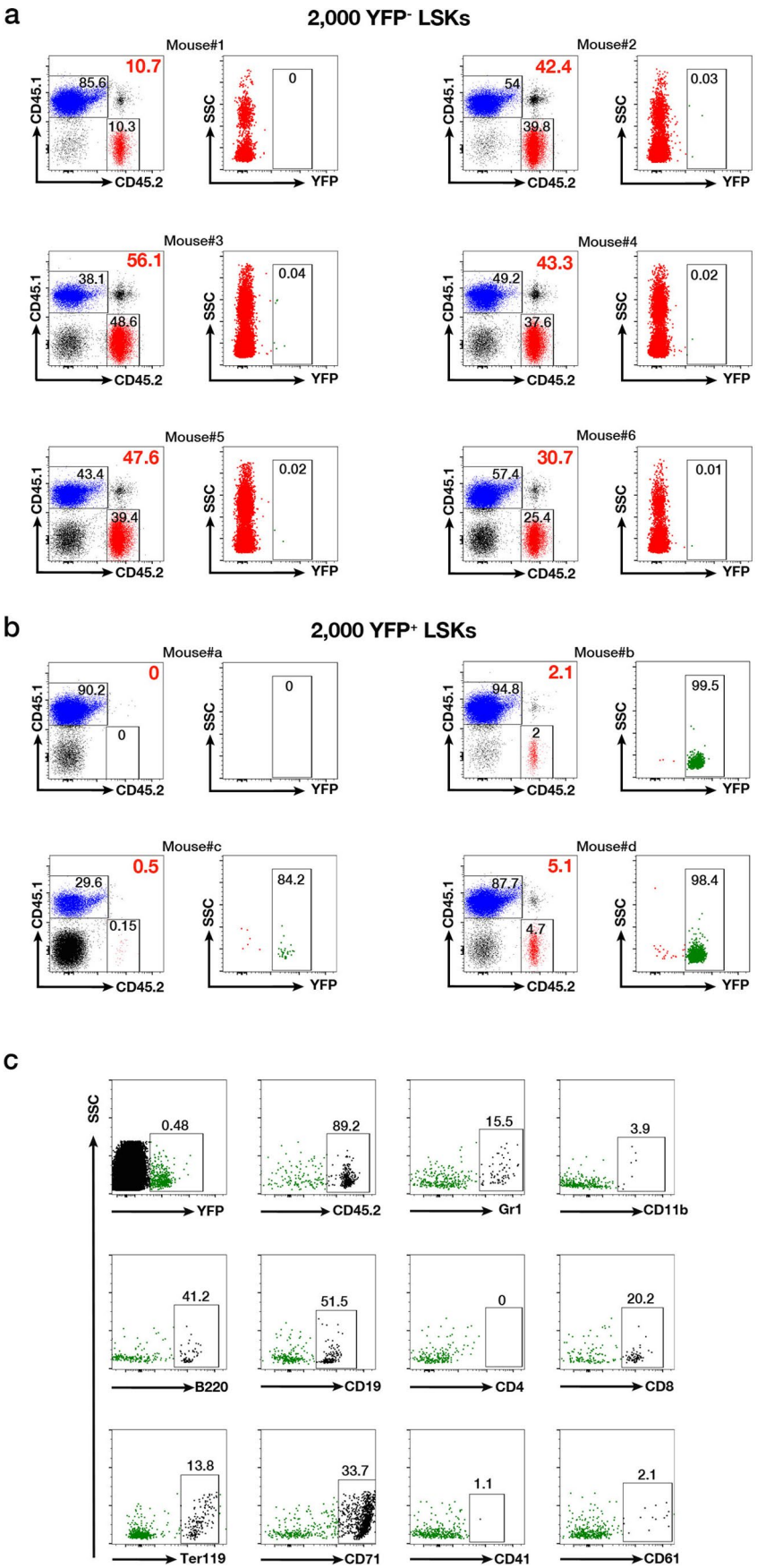

Extended Data Fig. 10 | See caption on next page.

Extended Data Fig. 10 | Long-term repopulation analysis in the peripheral blood of recipients transplanted either with YFP$^-$ or YFP$^+$ LSK cells. a, b, Flow cytometry analysis of circulating blood from 6 (**a**) and 4 (**b**) C57Bl/6-CD45.1 recipient mice at 11 weeks injected with 2,000 YFP$^-$ (**a**) or YFP$^+$ (**b**) LSK cells (C57Bl/6-CD45.2), respectively. Mice recipients transplanted with YFP$^-$ LSK cells displayed a more robust reconstitution than the ones transplanted with YFP$^+$ LSK cells. Of note, two mice in the LSK YFP$^+$ series died before two weeks post-injection. **c**, Back-gating within the GFP$^+$ population of the mononucleated bone marrow cells from mouse #d at 14 weeks of reconstitution. Dot plot representation of flow cytometry multilineage analysis showing Gr1 (granulocytes), CD11b (macrophages/monocytes), B220 and CD19 (B cells), CD4 (T cells), CD8 (T cells), Ter119 and CD71 (red cells), CD41 and CD61 (megakaryocytes) staining. The YFP population was more prominent in B220, CD19, CD71, Gr1 and CD8 fractions. Data in **a**-**c** representative of 2 independent experiments.